Energy & Buildings 328 (2025) 115191

Contents lists available at ScienceDirect

Energy & Buildings

journal homepage: www.elsevier.com/locate/enb

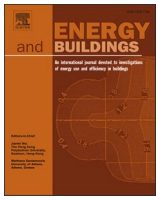

Developing a comprehensive method for integrating the thermal, optical and electrical properties of a complex fenestration system into building simulation software for building performance characterisation

Xue Li *, Yanyi Sun, Yupeng Wu *

Department of Architecture and Built Environment, Faculty of Engineering, The University of Nottingham, University Park, Nottingham NG7 2RD, United Kingdom

ARTICLE INFO

Keywords:
Building simulation
Building integrated PV (BIPV)
Crossed compound parabolic concentrator
Solar heat gain coefficient
Power output

ABSTRACT

To enhance energy conservation, indoor comfort, and mitigate greenhouse gas emissions in buildings, the design of glazed facades and window systems has seen substantial improvements. These enhancements result in increased thermal resistance while maintaining access to daylight and incorporating the use of renewable energy. Some of these glazing systems possess complex structures and PV cells, which present challenges in characterising their thermal, optical, and electrical properties for utilisation in building simulations. In this research, a comprehensive model has been developed to accurately predict the thermal, optical, and electrical properties of complex PV glazing systems, and a workflow has been developed to yield detailed thermal and energy performance predictions of these systems when applied to buildings. Using this approach, the thermal properties of complex PV glazing systems are obtained from a validated Computational Fluid Dynamics (CFD) combined ray-tracing model. The recursion algorithm, along with ray-tracing calculations, is used to determine their solar-optical properties. Additionally, a PV modelling algorithm has been developed to estimate their power output. All of these properties can be integrated into building simulation software, such as EnergyPlus, to assess the thermal and energy performance (e.g., solar heat gain coefficient and power output) of the complex PV glazing system when applied to a building. In this study, a Crossed Compound Parabolic Concentrator Photovoltaic (CCPC-PV) window is selected as an example of the complex PV glazing system, and a case study is conducted to investigate the annual energy performance (heating, cooling, lighting and power generation) of a typical cellular office room using the CCPC-PV window. The results demonstrate that the comprehensive model, simulating the CCPC-PV window within building simulation software, accurately characterises its thermal, optical, and electrical properties under London's climatic conditions. This high level of accuracy, with deviations of less than 5%, is of significant importance when simulating building energy performance with advanced glazing systems. Furthermore, the CCPC-PV window is more suitable for installation with a larger window-to-wall ratio (e.g., 64%), resulting in a 56.86% energy-saving percentage when compared to a similarly structured double-glazed window under London climate conditions.

1. Introduction

The building sector, which is regarded as one of the leading energy consumers around the world, uses up a significant proportion of approximately 40 % of the total primary energy in developed countries [1]. In addition, greenhouse gas emissions from the use of fossil fuels in buildings are a major driver of global warming [2]. Therefore, energy conservation and on-site renewable energy production have become the focus of energy policies and decision making for the future building design [3–5].

Compared to other building envelopes, the window system serves multiple functions, including thermal insulation, sound insulation, harnessing solar energy and daylight, weather protection, ventilation, and connecting to the outside [6,7]. However, the traditional window system is the thermally weakest part and around 60 % of energy loss would result from the window system through conduction, convection, and radiation heat transfer [8–10]. Additionally, they tend to lead to oversupply of daylight and solar heat in summer due to high transmittance particularly when used on south-facing façades [11]. To comprehensively enhance the thermal and optical performance of window systems while incorporating renewable energy into building design,

* Corresponding authors.
E-mail addresses: Xue.Li@nottingham.ac.uk (X. Li), Yupeng.Wu@nottingham.ac.uk (Y. Wu).

https://doi.org/10.1016/j.enbuild.2024.115191
Received 10 April 2024; Received in revised form 18 November 2024; Accepted 12 December 2024
Available online 17 December 2024

Nomenclature

ε	emissivity[-]
σ	Stefan-Boltzmann constant[W/m^2·K^4]
η	efficiency[-]
θ	solar incident angle[°]
φ	solar azimuth angle[°]
d	thickness[m]
E	long-wave radiation incident on window[W/m^2]
k	conductance of glass layer[W/m^2·K]
h	air film convective conductance[W/m^2·K]
S	radiation (short-wave and long-wave from zone internal sources) absorbed by surface[W/m^2]
t	surface temperature[℃]
T	air temperature[℃] also, transmittance[-]
R	reflectance[-]
A	absorptance[-] also, area[m^2]
P	electrical power[W]
f	fraction of the surface area with active solar cells[-]
G	incident solar radiation [W/m^2]

Subscripts

g	glass
e1	equivalent layer of air cavity with CCPC-PV structure
e2	equivalent layer of front three layers
e	exterior
i	interior
surf	surface
activ	active
pv	photovoltaic

Dimensionless numbers

Gr	Grashof number
Nu	Nusselt number
Pr	Prandtl number

Abbreviation

CFD	computational fluid dynamics
PV	photovoltaic
BIPV	building integrated photovoltaic
CCPC	crossed compound parabolic concentrator
CCPC-PV	crossed compound parabolic concentrator photovoltaic
LBNL	lawrence berkeley national laboratory
BSDF	bidirectional scattering distribution functions
STPV	semi-transparent photovoltaic
SAPM	sandia array performance model
SHGC	solar heat gain coefficient
VT	visible transmittance
PS-TIM	parallel slat transparent insulation material
ELFM	equivalent layer fenestration model
WWR	window-to-wall ratio

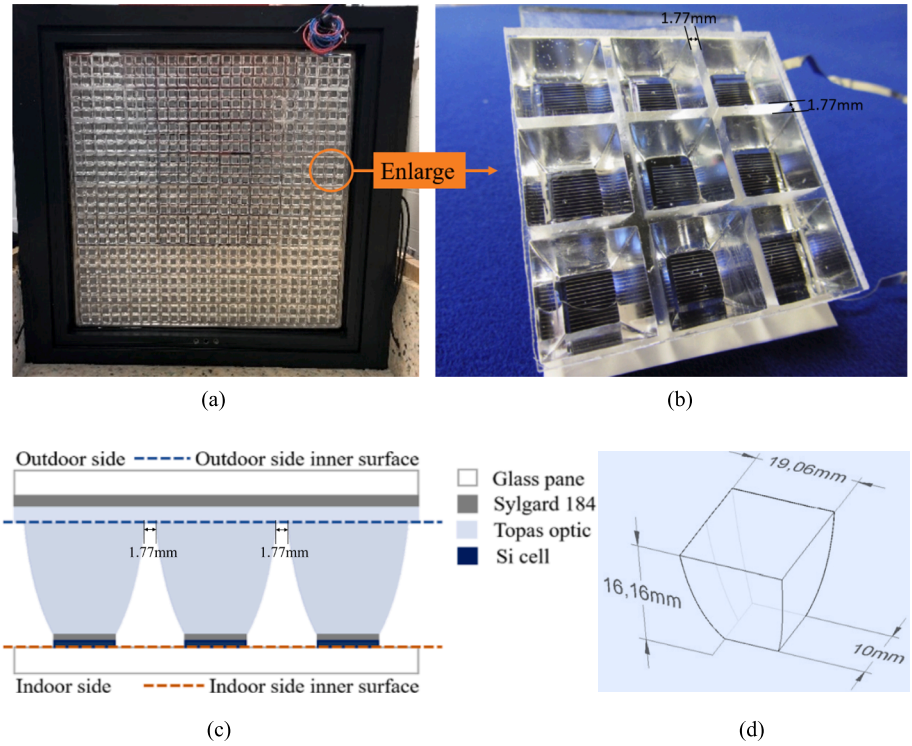

Fig. 1. Pictures of the (a) CCPC-PV window, (b) 3 × 3 CCPC-PV unit, (c) cross sectional view of the CCPC-PV window with detailed configuration, and (d) schematic sketch of a single CCPC optic.

innovative glazing systems with complex structures (e.g., solar optics) and PV cells [12–19] have been widely studied. For example, a Crossed Compound Parabolic Concentrator Photovoltaic (CCPC-PV) window system as shown in Fig. 1 has been designed, and its potential application to a building façade has been proposed [20–22]. The CCPC-PV window consists of 81 3 × 3 CCPC-PV modules (Fig. 1 (b)) arranged in a 9 × 9 matrix, sandwiched between two 4 mm-thick glass panes. The cross-sectional view of the CCPC-PV window in Fig. 1(c) illustrates the detailed configuration. From the outer layer to the inner layer, it consists of a 4 mm-thick float glass top pane, a 1.5 mm-thick silicone encapsulant

layer (Sylgard 184), a 2 mm-thick flat optic layer made of Topas (Polyolefin/Zeonex: COC Polymer), an air cavity containing 16.16 mm-thick CCPC optics made of Topas, and crystalline silicon solar cells (0.2 mm-thick and 1 cm^2-area for each cell) bonded with 0.2 mm-thick Sylgard. The horizontal and vertical pitches between two adjacent CCPC entry apertures are 1.77 mm, as shown in Fig. 1(b) and Fig. 1(c). Fig. 1 (d) illustrates the geometry of a single CCPC optic with a geometric concentration ratio of 3.6. The configuration is completed with a 4 mm-thick float glass bottom pane.

When exploring the building performance with this kind of complicated fenestration system integrated, numerical simulation methods tend to be used to investigate the detailed dynamic performance. Various building simulation tools, such as EnergyPlus, ESP-r, IES, TRNSYS and TAS, have been used to investigate the energy and/or daylight performance for buildings applied to various kinds of fenestration systems [23–30]. However, previous building simulation studies tend to separate the thermal and optical behaviours linked to the fenestration system. This separation is attributed to the complexity introduced by advanced glazing, which includes a complex window system structure, such as glazing with transparent insulation materials [31] and optical components [26,32]. The intricate structure of these windows poses a challenge for accurate simulation within most building simulation tools [33]. Currently, the available building energy simulation programs are not well-suited for accurately modelling these complex fenestration systems. Typically this is because they rely on simplified thermal and optical models to predict heat transfer and light transmittance, e.g., simple one dimensional methods are often used for the prediction of both heat transfer and light transmitted through fenestration systems [34]. Glazing systems with complex configurations are often characterised using pre-computed Solar Heat Gain Coefficients (SHGCs) and Visible Transmittances (VTs). Despite being determined using radiosity methods, these values are inadequate for representing the highly complex, angle-dependent interaction implicit when these systems are subjected to realistic time varying patterns of incident radiation [7]. The solar-optical properties of this kind of complex fenestration system can be represented by the Bidirectional Scattering Distribution Functions (BSDFs) within EnergyPlus. Sun et al.[7] used a Radiance tool genBSDF to generate BSDFs data for a Parallel Slat Transparent Insulation Material (PS-TIM) structure. The generated BSDFs data was then input into a utility, WINDOW, to generate a unified file of the complete system that contains effects of both the PS-TIM and glazing layers. This unified file was finally input into EnergyPlus to couple BSDFs data of the complex fenestration system into the building performance simulation. Moreover, McNeil et al.[35] verified the BSDFs data of a specular blind system and micro-perforated mesh generated from the genBSDF through the Tracepro simulation and goniophotometer measurement. Although the BSDF data produced by the Radiance tool genBSDF has been proven to accurately represent the solar-optical properties of the complex fenestration system, acquiring BSDF data remains a complex and time-consuming task [36]. In addition to BSDF data, very few studies have explored alternative methods for accurately characterising the solar-optical properties of complex fenestration systems and integrating them into building performance simulations. One such study by Tian et al. [36,37] developed a modified multiple nonlinear regression model to correlate the transmittance of a tilted dielectric Crossed Compound Parabolic Concentrator (dCCPC) skylight panel with sun positions and sky conditions. This model was integrated into building simulation software, EnergyPlus, using Grasshopper software. Using this method, they investigated the energy performance of the dCCPC skylight panel in various locations and climates. The results showed that the dCCPC skylight panel is more suitable for the cities having long hot period and the total energy saving could reach 13 %. For the cities with long cold seasons, it resulted in 1–5 % increase of the total annual energy consumption.

For complex fenestration systems with PV cells, integrating them into building performance simulations requires considering both the prediction of power output and the interactions among their electrical, thermal, and optical properties. Numerous studies have extensively investigated the building performance with traditional semi-transparent PV (STPV) windows [25,37–42]. For example, Sun et al.[37] investigated the building performance when a STPV glazing system (cadmium telluride) was installed with different designs. The Sandia Array Performance Model (SAPM) was used to predict the PV electrical performance while the BSDF data was used to optically characterise the CdTe window. Both SAPM and BSDF file were all input into a building simulation model within EnergyPlus. The simulation results showed that the application of the STPV glazing can result in considerable energy saving at a larger WWR ($\geq$45 %). Peng et al.[25,38,39] investigated the energy performance of various STPV (amorphous silicon) glazing systems installed on building façade. The optical properties, thermal conductivity, infrared emissivity of the PV module, as well as coefficients for SAPM were simulated or measured before the building energy performance simulation within Energyplus. The results showed that the average energy saving potential of the STPV glazing was around 30 % when compared to the commonly used insulating glass window in five representative climates in China. Innovative PV glazing systems with complex structures, such as those incorporating solar optics, exhibit fundamentally different electrical, thermal, and optical properties compared to traditional STPV glazing systems. The concentrating effect of solar optics highly depends on the solar incident angle. This results in higher solar radiation on PV cells at smaller angles (e.g., $\leq$30°) and lower radiation at larger angles (e.g., $\geq$50°), which directly impacts the electrical performance of innovative PV glazing systems. The SAPM built into EnergyPlus can be used to simulate the power generation of PV systems incorporating solar optics. However, it relies on a series of empirical relationships with numerous coefficients that require extensive testing to determine [38,43]. Furthermore, the presence of solar optics significantly complicates the mechanisms of heat transfer (conduction, convection, and radiation) and light transfer (transmittance, absorptance, and reflectance). Due to the complexity of the electrical, thermal, and optical properties of innovative PV glazing systems, very few studies have focused on methods to integrate these properties into building performance simulations, particularly considering their interactions. One example can be found in [26], where a comprehensive method was developed to model the dynamic electrical, thermal, and optical properties of an innovative BIPV smart window system. A PV power calculation algorithm, suitable for implementation in EnergyPlus, was developed to predict the on-site electricity generation of BIPV smart window systems in buildings. The thermal properties, specifically the U-value, were determined in accordance with the European Standard EN 673:2011[44]. The BSDF data, which is accurate but challenging to obtain as previously mentioned, was used to optically characterise the BIPV smart window. These properties were ultimately integrated into a building performance simulation model to assess their impact on building energy performance and visual comfort. However, examining the interactions between various window properties in this study remains relatively challenging.

Based on the literature review, it is evident that accurately integrating the thermal, optical, and electrical properties of fenestration systems with complex structures and PV cells, such as the CCPC-PV window, into existing building simulation software remains a significant challenge. To address this issue, this study introduces a method that offers a comprehensive representation of complex PV window systems applied to buildings. The approach differs from previous studies through the inclusion of a comprehensive model to characterise the thermal, optical, and electrical properties of the complex PV window system within the existing building simulation software, EnergyPlus. As an example, the CCPC-PV window is selected as the complex PV window in this study. The Computational Fluid Dynamics (CFD) combined ray-tracing method is used to determine its thermal properties, while the recursion algorithm combined ray-tracing calculation is used to obtain its solar-optical properties. Furthermore, window system output is

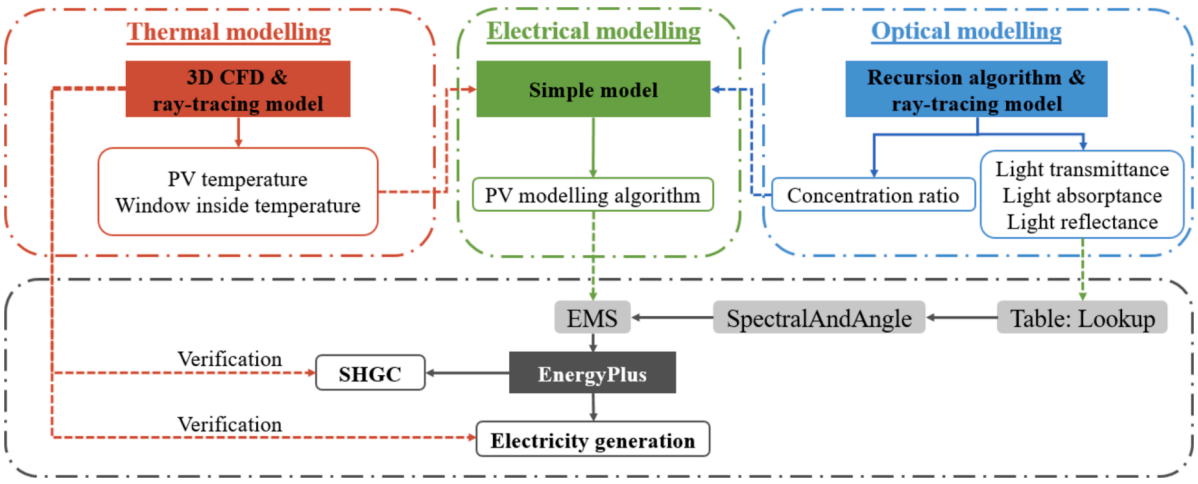

Fig. 2. Flowchart of coupling thermal, optical and electrical properties of the CCPC-PV window into window performance simulation within EnergyPlus.

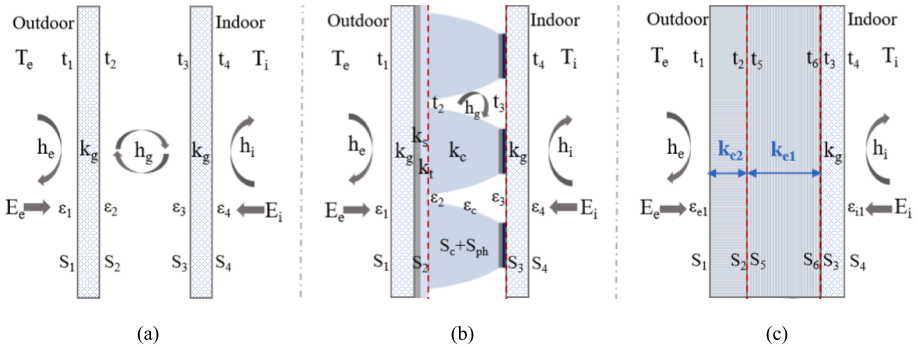

Fig. 3. Window heat balance for (a) double-glazed model, (b) CCPC-PV window original model and (c) CCPC-PV window Equivalent Layer Fenestration Model (ELFM).

estimated using a PV modelling algorithm. The thermal, optical, and electrical properties obtained from the above models are input into building simulation software, EnergyPlus, to predict the thermal and energy performance of the CCPC-PV window, such as the Solar Heat Gain Coefficient (SHGC) and power output when applied to a building. In the end, a case study investigates the annual energy performance (heating, cooling, lighting, and power generation) of a typical cellular office room using the CCPC-PV window with the previously mentioned window integration method under London climate conditions. The proposed research method for integrating complex PV window systems into building simulation software enables to observe the inter-relationship between its thermal, optical, and electrical properties. It also serves as a reference for other researchers planning to conduct building performance simulations with complex (PV) fenestration systems.

2. Methodology

This section presents a workflow that incorporates thermal, optical, and electrical characteristics of a complex PV fenestration system into building simulation software, EnergyPlus. The CCPC-PV window is used to illustrate how this method might be used. The developed holistic method consists of four major blocks as shown in Fig. 2:

(1) A fenestration thermal model where a three-dimensional Computational Fluid Dynamics (CFD) combined ray-tracing simulation has been used to investigate the thermal properties, such as the window temperature and PV temperature of the CCPC-PV window under different weather conditions (i.e., different solar radiation intensity and solar incident angle).
(2) A fenestration optical model where the recursion algorithm combined ray-tracing calculation has been used to obtain optical properties, such as the light transmittance and absorptance of the CCPC-PV window at different solar incident angles.
(3) An electrical model where the 'Simple' model in EnergyPlus has been modified based on the temperature coefficient of the PV cell and concentrating ratio of the CCPC-PV window to predict the power output.
(4) A building energy simulation where the thermal, optical, and electrical characteristics of the fenestration system obtained from previous thermal, optical, and electrical models are applied within EnergyPlus to obtain the window thermal and energy performance under imposed climatic conditions.

In the end, simulation results within EnergyPlus, such as the light transmittance, solar absorptance, window temperature, window inward convection, radiation, and secondary heat flux to the indoor space, SHGC and power output of the CCPC-PV window are compared using a validated 3D CFD combined ray-tracing method under different weather conditions in London (latitude, longitude of 51°32′28″N, 0°7′41″W, respectively) to ensure the obtained properties from individual models are properly coupled into the building performance simulation within EnergyPlus. The theories and outcomes of each stage are described in the following sections.

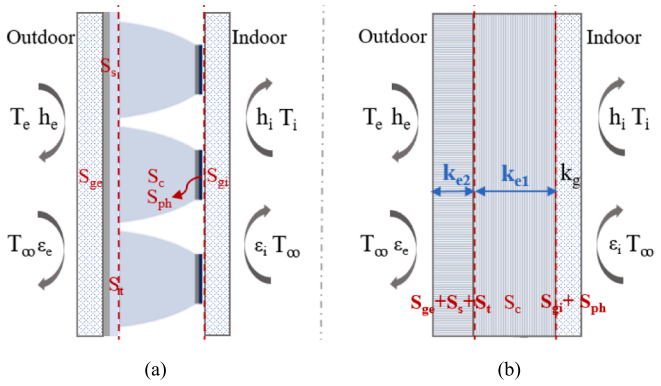

Fig. 4. Boundary conditions for (a) original CCPC-PV window model and (b) ELFM.

Table 1
Material properties of the ELFM [31,47].

Material	Property	Unit	Value
Glass pane	Conductivity	W/m· K	1.4
Sylgard 184	Conductivity	W/m· K	0.16
Topas (flat)	Conductivity	W/m· K	0.20
Air cavity with CCPC-PV	Equivalent thermal conductivity	W/m· K	0.185
Front three layers	Equivalent thermal conductivity	W/m· K	0.337

Table 2
Different outdoor boundary conditions for the thermal modelling.

Boundary conditions	Unit	Value
Outdoor air temperature	℃	−2, 10, 20, 30
Outside convective heat transfer coefficient	W/m^2•K	0, 5, 10, 15, 20
Solar radiation on window outside surface	W/m^2	0, 200, 400, 600, 800
Incident angle	°	0, 20, 40, 60, 80

Table 3
Window inside surface temperatures of the CCPC-PV window model and its ELFM.

Boundary conditions	Unit	Value	Window inside surface temp. of CCPC-PV window model (℃)	Window inside surface temp. of ELFM (℃)	Deviation (%)
Outdoor air temperature	℃	−2	49.15	50.84	3.44 %
		10	52.99	54.68	3.19 %
		20	56.22	57.90	2.99 %
		30	59.48	61.19	2.87 %
Outdoor surface heat transfer coefficient	W/m^2•K	0	64.96	66.65	2.60 %
		5	61.42	63.12	2.77 %
		10	59.46	61.18	2.89 %
		15	58.24	60.01	3.04 %
		20	57.40	59.21	3.15 %
Solar radiation	W/m^2	0	27.07	27.13	0.22 %
		200	35.69	36.24	1.54 %
		400	44.07	45.16	2.47 %
		600	52.32	54.12	3.44 %
		800	60.79	62.40	2.65 %
Incident angle	°	0	60.13	61.86	2.88 %
		20	58.31	59.97	2.85 %
		40	50.40	51.50	2.18 %
		60	32.54	32.89	1.08 %
		80	27.56	27.70	0.51 %

Table 4
PV temperature of the CCPC-PV window model and window inside surface temperature of its ELFM.

Boundary conditions	Unit	Value	PV temp. of CCPC-PV window model (℃)	Window inside surface temp. of ELFM (℃)	Temp. diff. (℃)
Outdoor air temperature	℃	−2	51.95	50.84	1.11
		10	56.03	54.68	1.35
		20	59.45	57.90	1.55
		30	62.91	61.19	1.72
Outdoor surface heat transfer coefficient	W/m^2•K	0	68.73	66.65	2.08
		5	64.97	63.12	1.85
		10	62.89	61.18	1.71
		15	61.59	60.01	1.58
		20	60.70	59.21	1.49
Solar radiation	W/m^2	0	27.23	27.13	0.10
		200	36.67	36.24	0.43
		400	45.87	45.16	0.71
		600	54.97	54.12	0.85
		800	64.34	62.40	1.94
Incident angle	°	0	63.60	61.86	1.74
		20	61.58	59.97	1.61
		40	52.78	51.50	1.28
		60	33.07	32.89	0.18
		80	27.74	27.70	0.04

2.1. *Thermal properties of the CCPC-PV window for coupling into building performance simulation*

Through understanding the heat transfer method to predict the thermal and energy performance of the glazing system within EnergyPlus, a fenestration model representing the CCPC-PV window is proposed to be coupled into the building performance simulation. In addition, thermal properties of the above fenestration model are investigated using a 3D CFD combined ray-tracing method under different weather conditions in London.

2.1.1. *Glazing heat balance equations in EnergyPlus*

EnergyPlus, a widely adopted building performance simulation software, calculates the indoor heating and cooling by solving the heat balance algorithms [45]. When solving the heat transfer through glazing systems, it is assumed as a layer-by-layer structure with one-dimensional heat transfer. The surface temperature of the multilayer glazing system is determined by solving the heat balance equation on each surface [43]. Fig. 3 (a) shows variables involving in the heat balance equation for each surface in a double-glazed system. The heat balance equation for each glazing unit's surface can be written as Eq. (1) to (4) [43].

$$E_e\varepsilon_1 - \varepsilon_1\sigma t_1^4 + k_g(t_2 - t_1) + h_e(T_e - t_1) + S_1 = 0 \quad (1)$$

$$k_g(t_1 - t_2) + h_g(t_3 - t_2) + \sigma\frac{\varepsilon_2\varepsilon_3}{1-(1-\varepsilon_2)(1-\varepsilon_3)}(t_3^4 - t_2^4) + S_2 = 0 \quad (2)$$

$$k_g(t_4 - t_3) + h_g(t_2 - t_3) + \sigma\frac{\varepsilon_2\varepsilon_3}{1-(1-\varepsilon_2)(1-\varepsilon_3)}(t_2^4 - t_3^4) + S_3 = 0 \quad (3)$$

$$E_i\varepsilon_4 - \varepsilon_4\sigma t_4^4 + k_g(t_3 - t_4) + h_i(T_i - t_4) + S_4 = 0 \quad (4)$$

where, E_e and E_i are exterior and interior long-wave radiation incident on window, W/m^2. ε_i is emissivity of face i (i = 1, 2, 3, 4 for a double-glazed window). σ is Stefan-Boltzmann constant, W/m^2·K^4. t_i is temperature of face i, K. k_g is conductance of glass layer, W/m^2·K. h_e and h_i are external and internal air film convective conductance, W/m^2·K. T_e and T_i are exterior and interior air temperature, K. S_i is radiation (short-wave, and long-wave from zone internal sources) absorbed by face i, W/m^2.

For a double-glazed window unit, the heat transfer occurs into the gas cavity between two glazing panes consists of convective and radia-

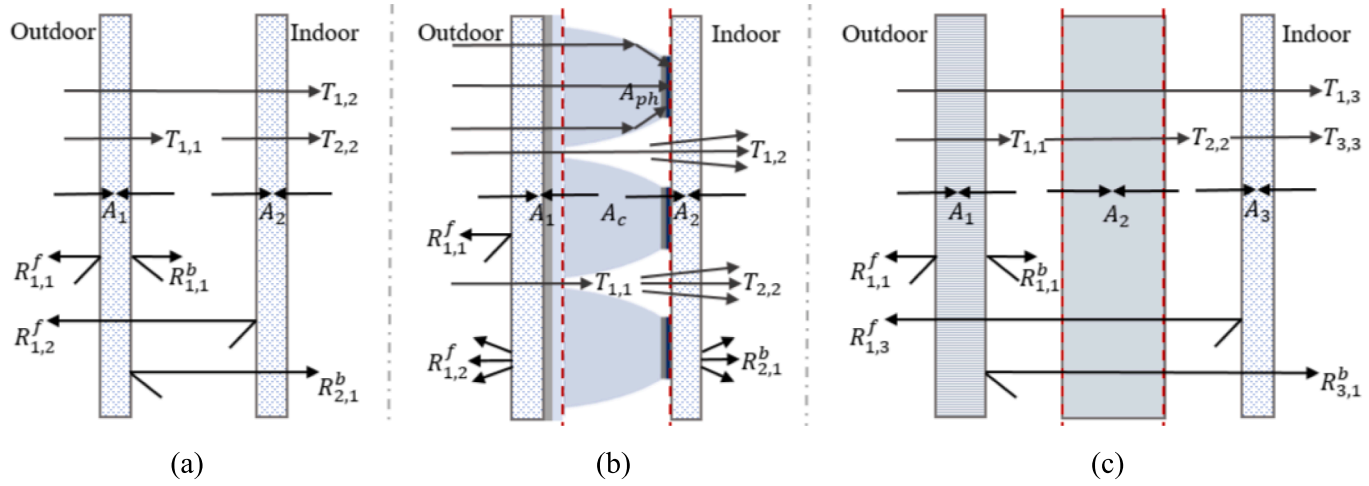

Fig. 5. Schematic of transmission, reflection, and absorption of solar radiation within a (a) double-glazed model, (b) CCPC-PV window model, and (c) its ELFM.

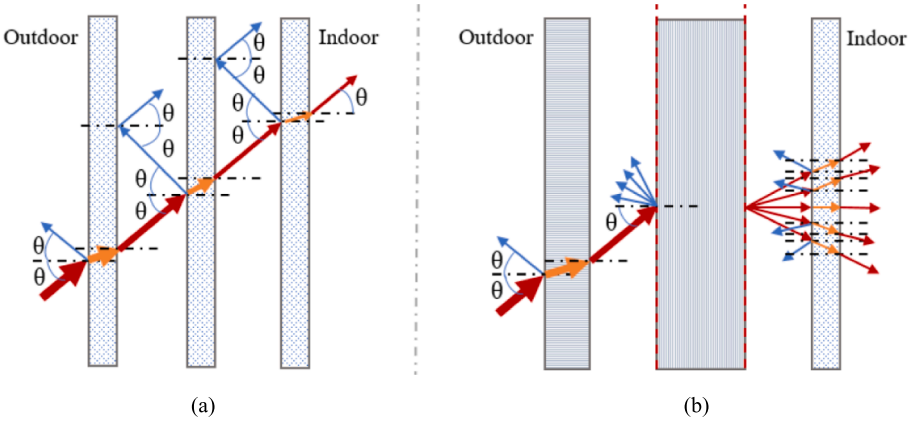

Fig. 6. Light transmission through the (a) multilayer glazing system and (b) ELFM under θ incident angle.

tive heat transfer. The convective heat transfer coefficient (h_g) is represented by the non-dimensional Nusselt (Nu) number, which is affected by three dimensionless parameters: the Prandtl (Pr), Grashof (Gr) number of the gap fluid as well as the aspect ratio (geometry) of the cavity [31]. While the strength of radiative heat transfer across the gas cavity is determined by the emissivity of the two glazing surfaces that enclose it and view factors between them. When a complex structure, such as an array of CCPC optics and PV cells exists into the gas cavity between two glazing panes (Fig. 3(b)), heat transfer between the panes includes the following:

(1) Convective heat transfer: Convection arises as air circulates within the cavity surrounding the CCPC-PV structure and bounded by the two glazing panes.
(2) Radiative heat transfer: Radiative heat transfer primarily occurs between the inner surfaces of the glass panes and the CCPC optic surfaces.
(3) Conductive heat transfer: Conductive heat transfer mainly occurs through the solid components of the CCPC-PV structure, specifically through the CCPC optics and PV cells, which are in direct contact with each other.
(4) Additional heat sources: In addition to the convective, radiative, and conductive heat transfer processes mentioned above, the CCPC optics absorb a portion of the solar radiation entering the window, while the PV cells generate heat as a byproduct of converting solar energy into electricity. These heat sources increase the total thermal load and are transferred throughout the entire window system via conduction, convection, and radiation.

Based on the above analysis, it can be seen that the heat transfer becomes much more complicated when complex structures and PV cells exist into the air cavity between two glazing panes. To accurately simulate the heat transfer through the CCPC-PV window within EnergyPlus, the air cavity with CCPC optics and PV cells (the part between two dotted lines in Fig. 3 (b)) could be assumed as one equivalent layer with an equivalent thermal conductivity and equivalent heat source term as shown in Fig. 3 (c). The equivalent thermal conductivity, K_{e1}, represents the combined conductive, convective, and radiative heat transfer through the air cavity with a CCPC-PV structure into the CCPC-PV window. For the purpose of the heat balance calculation, the equivalent heat source, which consists of the solar energy absorbed by CCPC-solids and the heat released by the PV power generation, was split equally and applied to the outdoor side inner surface (S_5) and indoor side inner surface (S_6). Similarly, the front three flat layers were also assumed as one equivalent layer with an equivalent thermal conductivity (K_{e2}) representing the total conductive heat transfer through it and an equivalent heat source term representing the total solar energy absorbed by it. The equivalent heat source term for the front three layers was also split equally and applied to the outdoor side surface (S_1) and outdoor side inner surface (S_2). Based on the above analysis, an 'Equivalent Layer Fenestration Model (ELFM)', which consists of an equivalent layer for the front three layers, an equivalent layer for the air cavity containing a CCPC-PV structure and an indoor glass layer as

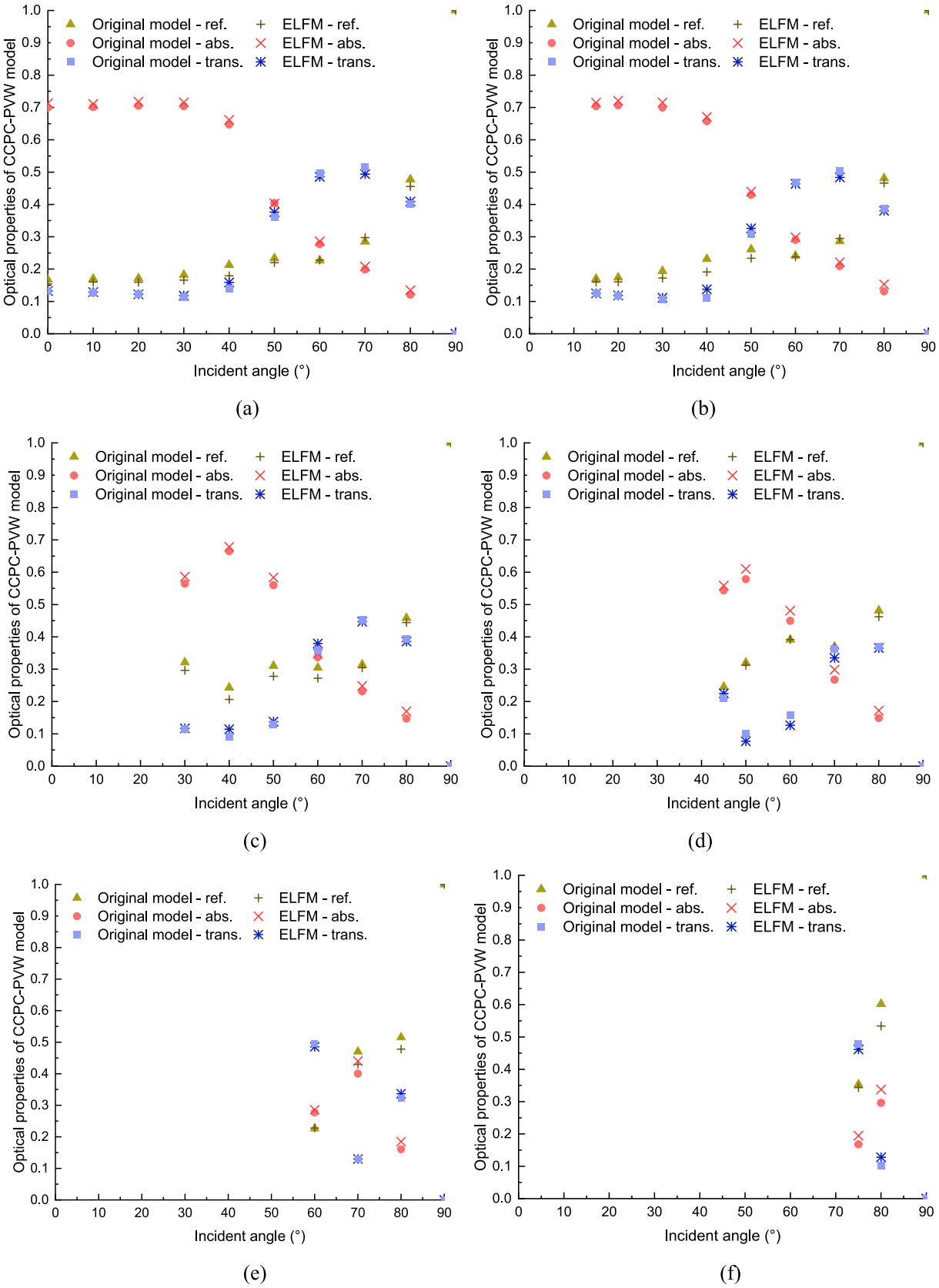

Fig. 7. Light transmittance, absorptance and reflectance of the original model and ELFM under direct solar radiation condition for rays from (a) 172.5°-187.5° azimuth angles, (b) 157.5°-172.5°& 187.5°-202.5° azimuth angles, (c) 142.5°-157.5° & 202.5°-217.5° azimuth angles, (d) 127.5°-142.5° & 217.5°-232.5° azimuth angles, (e) 112.5°-127.5° & 232.5°-247.5° azimuth angles and (f) 90°-112.5° & 247.5°-270° azimuth angles.

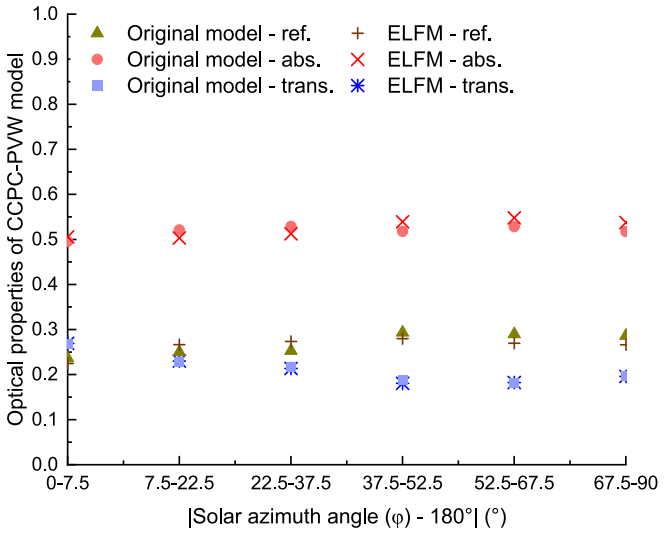

Fig. 8. Light transmittance, absorptance and reflectance of the CCPC-PV window model and its ELFM under diffuse solar radiation condition.

shown in Fig. 3 (c) was proposed. The ELFM can be used to represent the CCPC-PV window and be coupled to the building performance simulation within EnergyPlus. The heat balance equations for each surface of the ELFM can be written as Eq. (5) to (10). Methods to investigate the thermal, optical, and electrical properties of the above ELFM and the methods to couple the ELFM into the building simulation software to conduct the building performance simulation are illustrated in the following sections.

$$E_e\varepsilon_1 - \varepsilon_1\sigma t_1^4 + k_{e2}(t_2 - t_1) + h_e(T_e - t_1) + S_1 = 0 \quad (5)$$

$$k_{e2}(t_1 - t_2) + S_2 = 0 \quad (6)$$

$$k_{e1}(t_6 - t_5) + S_5 = 0 \quad (7)$$

$$k_{e1}(t_5 - t_6) + S_6 = 0 \quad (8)$$

$$k_g(t_4 - t_3) + S_3 = 0 \quad (9)$$

$$E_i\varepsilon_4 - \varepsilon_4\sigma t_4^4 + k_g(t_3 - t_4) + h_i(T_i - t_4) + S_4 = 0 \quad (10)$$

2.1.2. *Method for acquiring thermal properties*

In this section, a three-dimensional finite volume model combined with a ray-tracing model, developed using the commercial CFD software package FLUENT and commercial software TracePro, has been employed to investigate thermal properties of the ELFM. The ray-tracing model enables the calculation of transmitted, reflected and absorbed fraction of solar irradiation for different elements into the ELFM. The resulting absorbed components of solar irradiation (including the solar energy absorbed by each element and solar heat released by PV power generation) were transferred as volume heat sources then input into the CFD model as one of the boundary conditions. The thermal modelling results for the ELFM, such as the average window inside surface temperature and average PV temperature, were compared with that of the original CCPC-PV window under different weather conditions in London.

A validated CFD model has already been established to investigate thermal properties of the CCPC-PV window (e.g., PV temperature, window temperature and SHGC) in our recent work by Li et al (2023) [46] and the boundary conditions can be found in Fig. 4 (a). The CFD model for the ELFM could be modified based on that of the original CCPC-PV window using the concept of equivalent layers as described in the last section and the boundary conditions can be found in Fig. 4 (b). The equivalent thermal conductivity (K_{e2}) of the front three layers (k_g, k_s and k_t in Fig. 4 (b)) was calculated using Eq. (11). As the conductive heat transfer dominants the heat transfer mechanism into the air cavity with CCPC-PV structure between two glazing panes as mentioned in [42], the equivalent thermal conductivity (K_{e1}) was not sensitive to the changing temperature conditions and was averaged as 0.185 W/m·K across all temperature conditions. The thermal conductivities for the other materials can be found in Table 1.

A validated ray-tracing model was also established to simulate the solar energy absorbed by each solid element and PV cells in the original CCPC-PV window as described in our recent work by Li et al (2023) [46]. The equivalent heat source for front three layers is the sum of the solar energy absorbed by the exterior glass, sylgard layer and flat topas layer. Instead of splitting the heat source equally then applied to two faces of a layer as those used for the glazing heat balance calculation in EnergyPlus, the equivalent heat source term ($S_{ge} + S_s + S_t$) was transformed as a volume heat source and then input into the corresponding equivalent solid layer as one of the boundary conditions (Fig. 4 (b)). Similarly, the sum of the solar energy absorbed by the CCPC-solids (S_c) and heat released by PV power generation (S_{ph}) should also be converted as a

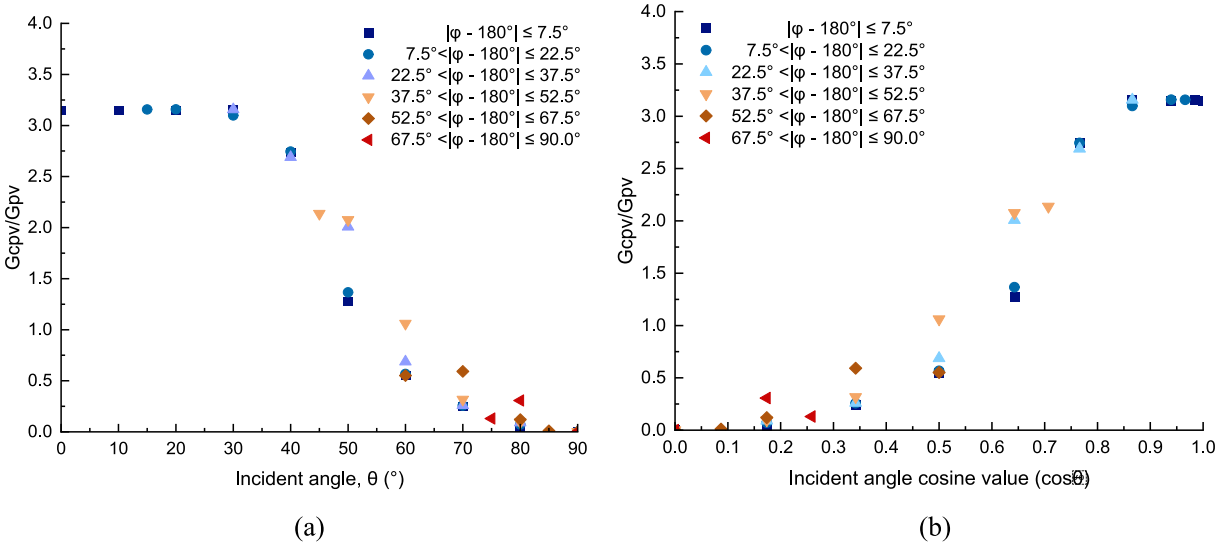

Fig. 9. Relation between the concentrating effect (G_{cpv}/G_{pv}) and (a) solar incident angle (θ) and (b) cosine value of the incident angle ($cos\theta$) for solar rays from different azimuth angle (φ) range.

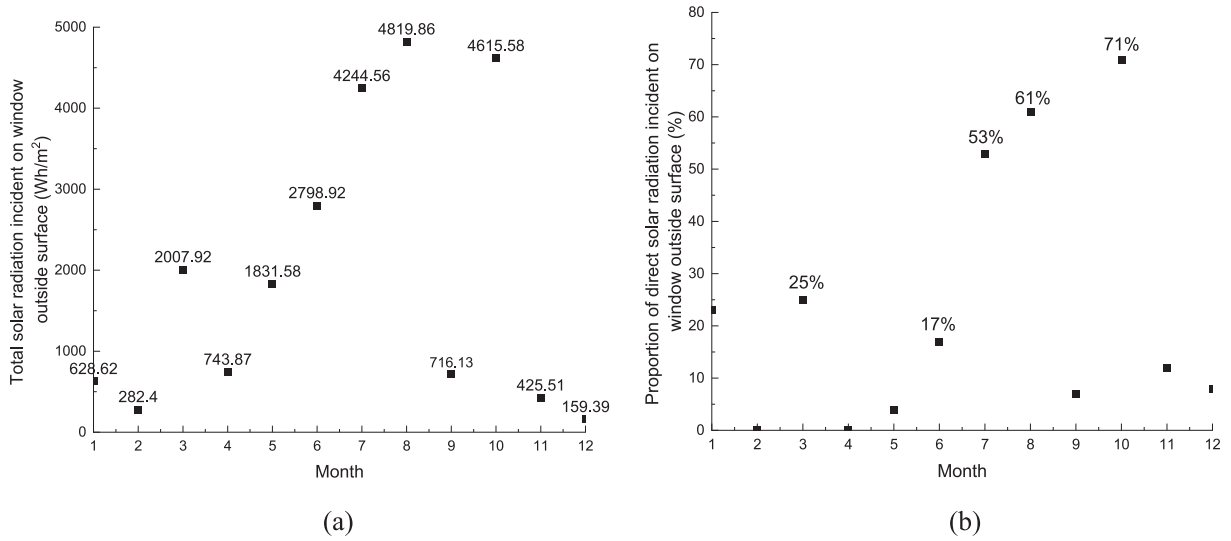

Fig. 10. (a) Total solar radiation incident on window outside surface per window area and (b) proportion of direct solar radiation incident on window outside surface on 22nd of each month.

volume heat source to be input into the middle equivalent layer in the numerical model. However, the volume of the equivalent layer for the air cavity with CCPC-PV units is much larger than that of small PV cells, which would lead to a large deviation of the inside surface temperature between the ELFM and original CCPC-PV window model. Therefore, the solar heat released by PV power generation was incorporated into the indoor glass layer rather than the middle equivalent layer.

$$K_e = \frac{d_g + d_s + d_t}{\frac{d_g}{K_g} + \frac{d_s}{K_s} + \frac{d_t}{K_t}} \tag{11}$$

where, d_g, d_s, and d_t are the thickness of exterior glass, sylgard layer and flat topas layer, m, K_g, K_s, and K_t are the thermal conductivity of exterior glass, sylgard layer and flat topas layer, W/m• K.

Fig. 4 also shows the combined convective and radiative boundary conditions were applied for window indoor and outdoor sides. The convective heat transfer is determined by the air temperatures (T_e and T_i) and convective heat transfer coefficients (h_e and h_i). While the radiative heat transfer is determined by the emissivity (ε_e and ε_i) and radiation temperature ($T\infty$). As the thermal property of the window is highly affected by changing outdoor environmental conditions, the simulation was conducted under different outside boundary conditions as shown in Table 2, which includes all the weather conditions according to an IWEC (International Weather for Energy Calculation) weather file for London (latitude 51.5°N and the longitude 0°W). The indoor side boundary conditions (24) ℃ air temperature, 3.6 W/m^2• K surface convective heat transfer coefficient and 0.84 emissivity) was kept unchanged across all of simulations.

2.1.3. Thermal modelling of window inside surface temperature

This section presents simulation results for the window inside surface temperature of the ELFM and the results were also compared with that of the original CCPC-PV window model. Table 3 listed the window inside surface temperature of the CCPC-PV window model and its ELFM under different weather conditions. Compared to outdoor air temperature and convective heat transfer coefficients, solar radiation and solar incident angles have a greater impact on the interior surface temperature of both the CCPC-PV window model and its ELFM. Deviations of the window inside surface temperature between the original model and its ELFM are within 4 % across all weather conditions. Therefore, the ELFM developed in this study is relatively accurate to simulate thermal properties of the CCPC-PV window.

2.1.4. Thermal modelling of PV temperature

The PV temperature of the ELFM could be obtained from the relation between the PV temperature of the CCPC-PV window model and window inside surface temperature of the ELFM. Table 4 shows simulation results under different weather conditions and the average temperature difference between the PV temperature of the CCPC-PV window model and window inside surface temperature of the ELFM across the weather conditions in London was calculated as 1.23 ℃ (Eq. (12)), which was then used to predict the power output of the CCPC-PV window in **Section 2.3.2**.

$$t_{pv} = t_{si} + 1.23 \tag{12}$$

where, t_{si} is the window inside surface temperature of the ELFM, ℃. t_{pv} is the PV temperature of the CCPC-PV window model, ℃.

2.2. Optical properties of the CCPC-PV window for coupling into building performance simulation

This section introduces fundamental theories of the light transmission method to predict optical properties of the glazing system within EnergyPlus first. Then a method of the recursion algorithm [48,49] combined with the ray-tracing simulation has been used to investigate the optical properties of the ELFM at different solar incident angles.

2.2.1. Glazing light transmission equations in EnergyPlus

The light transmission method for a multilayer glazing system within EnergyPlus is similar to the heat transfer method as described in **Section 2.1.1**. A layer-by-layer structure with one-dimensional light transmission was also assumed when solving for light transmission through the multilayer glazing system. Optical properties of the whole multilayer glazing system were estimated from optical characteristics of individual panes into the system. While optical characteristics of individual panes are given by the transmittance (T), front reflectance (R^f) and back reflectance (R^b) [43]. Fig. 5 (a) shows variables involving in the light transmission through different layers into a double-glazed system. To calculate the total transmittance, front/back reflectance and absorptance of a double-glazed unit, recursion relations as described in Eq. (13) – (16) were solved [43]. These relations also account for multiple internal reflections within the glazing system.

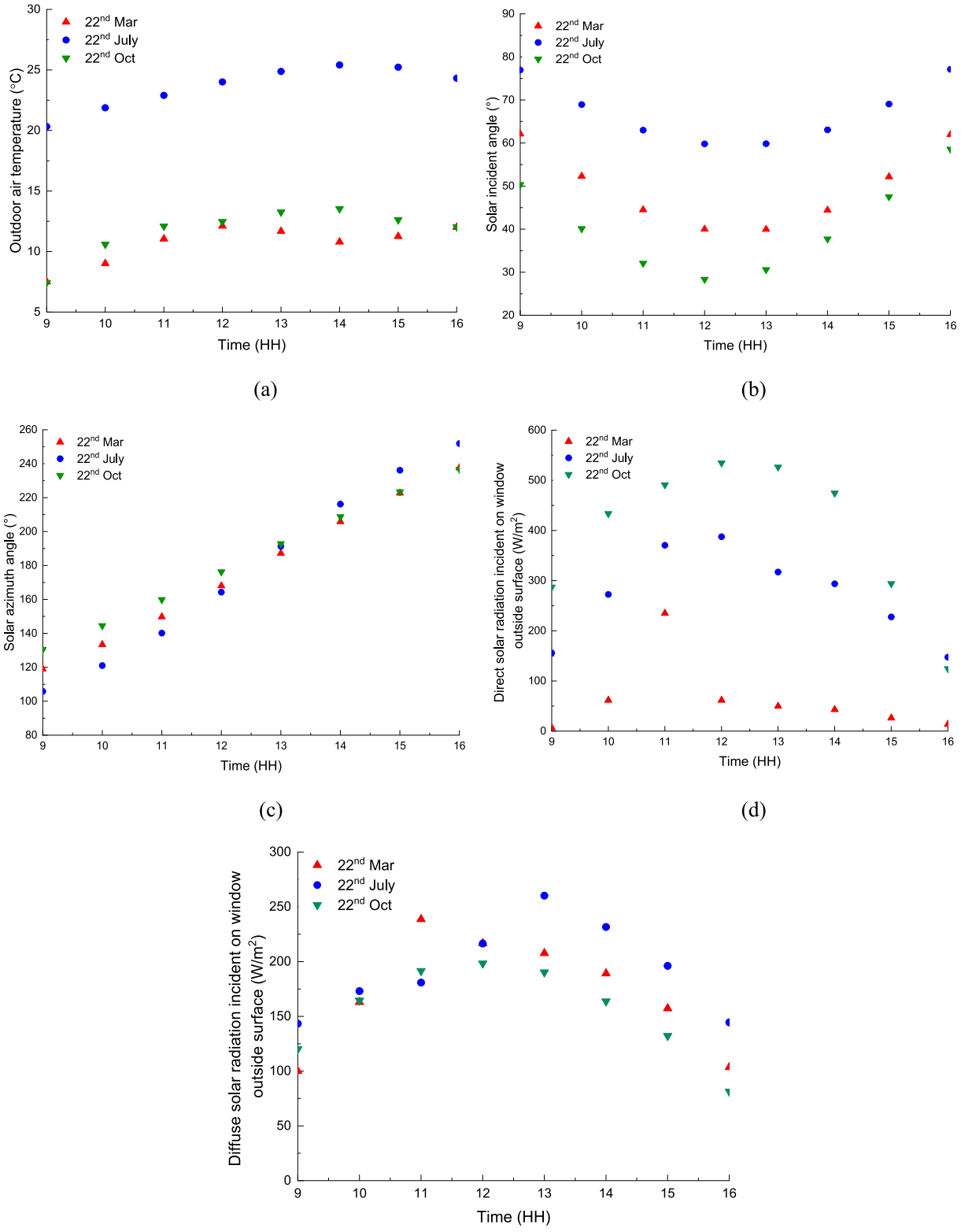

Fig. 11. (a) Outdoor air temperature, (b) solar incident angle, (c) solar azimuth angle, (d) direct and (e) diffuse solar radiation incident on window outside surface on 22nd Mar, 22nd July, and 22nd Oct.

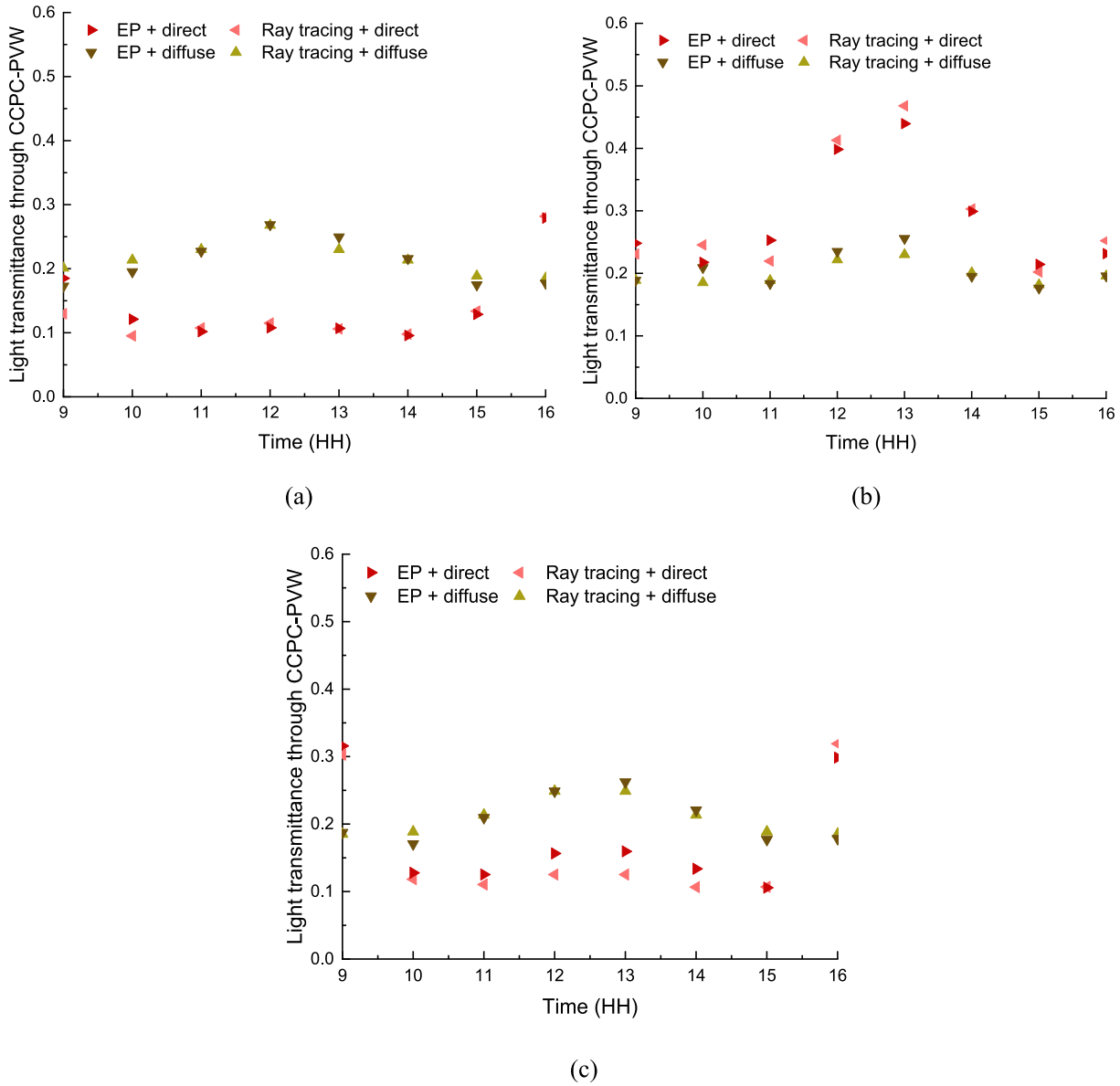

Fig. 12. Direct and diffuse light transmittance on (a) 22nd Oct, (b) 22nd July, and (c) 22nd Mar.

$$T_{1,2} = \frac{T_{1,1}T_{2,2}}{1 - R^f_{2,2}R^b_{1,1}} \tag{13}$$

$$R^f_{1,2} = R^f_{1,1} + \frac{T^2_{1,1}R^f_{2,2}}{1 - R^f_{2,2}R^b_{1,1}} \tag{14}$$

$$R^b_{2,1} = R^b_{2,2} + \frac{T^2_{2,2}R^b_{1,1}}{1 - R^b_{1,1}R^f_{2,2}} \tag{15}$$

$$A^f_{1,2} = \left(1 - T_{1,1} - R^f_{1,1}\right) + T_{1,1}R^f_{2,2}\left(1 - T_{1,1} - R^b_{1,1}\right) + \frac{T_{1,1}(1 - T_{2,2} - R^f_{2,2})}{1 - R^f_{2,2}R^b_{1,1}} \tag{16}$$

where, $T_{i,j}$ is transmittance through glass layers i ($i = 1, 2$) to j ($j = 1, 2$). $R^f_{i,j}$ is front reflectance from glass layers i to j. $R^b_{j,i}$ is back reflectance from glass layers j to i. $A^f_{i,j}$ is front absorptance through glass layers i to j.

When a complex structure, such as an array of CCPC-PV units existing into the air cavity between two glazing panes (Fig. 5 (b)), one-dimensional light transmission through the air cavity is interrupted because of the complex light behaviour into the CCPC optics. The light will be reflected and transmitted with different angles after through the air cavity with a CCPC-PV structure. In addition, the existing of PV cells indicates that a portion of light rays is absorbed by PV cells after the CCPC concentrating, rather than participating in the light transmission. The concept of equivalent layer in the thermal modelling process (**Section 2.1**) was also used to represent the complex light transmission into the air cavity with a CCPC-PV structure. As shown in Fig. 5 (c), $T_{i,i}$, $A_{i,i}$ and $R_{i,i}$ represent the light transmittance, absorptance and reflectance of the equivalent layer for front three flat layers ($i = 1$), equivalent layer for the air cavity with a CCPC-PV structure ($i = 2$) and indoor glass layer ($i = 3$). The total transmittance, front/back reflectance and absorptance of the ELFM could be calculated using following recursion relations as described in Eq. (17) – (20) [43].

$$T_{1,3} = \frac{T_{1,2}T_{3,3}}{1 - R^f_{3,3}R^b_{2,1}} \tag{17}$$

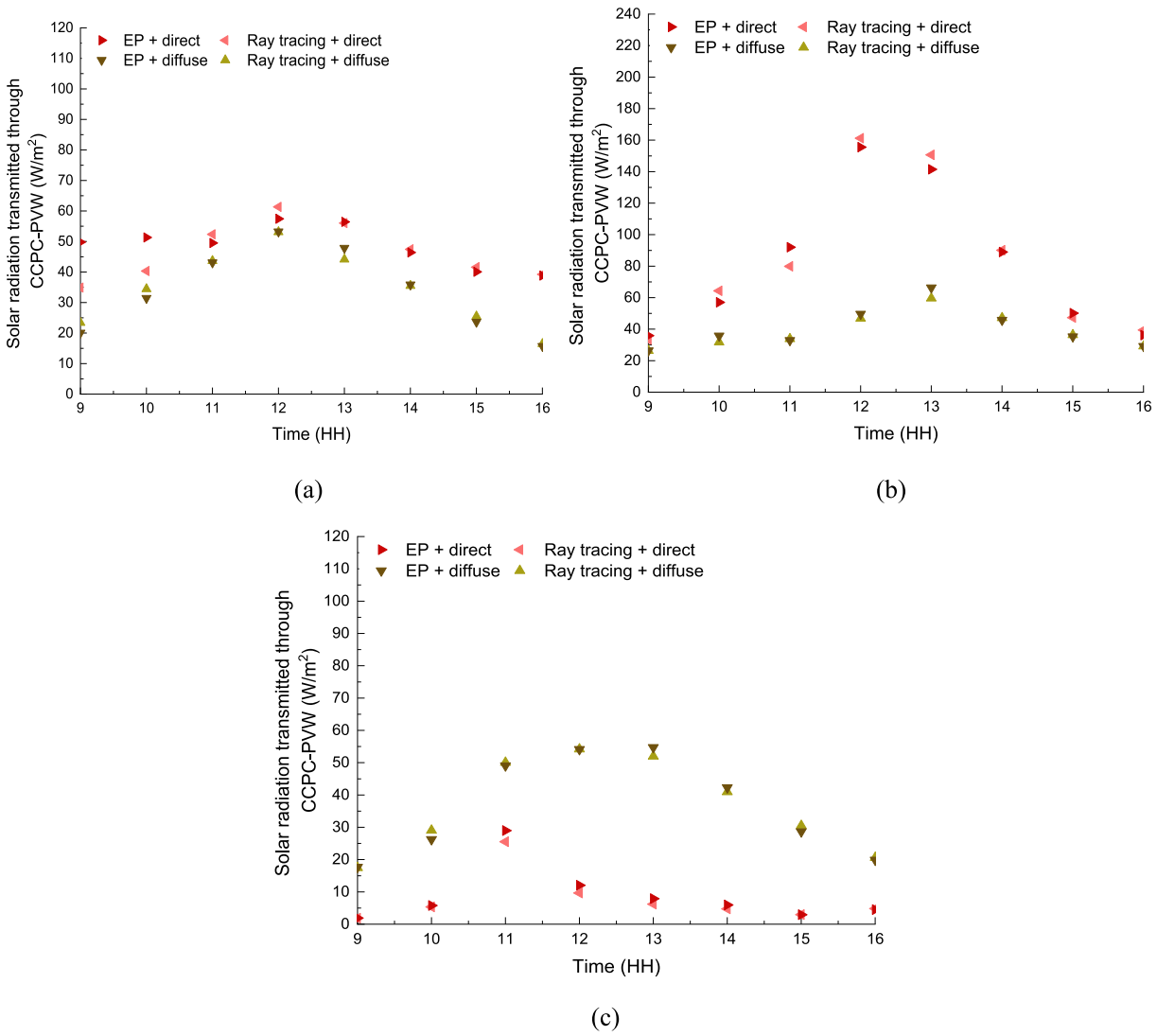

Fig. 13. Transmitted direct and diffuse solar radiation rate on (a) 22nd Oct, (b) 22nd July, and (c) 22nd Mar.

$$R^f_{1,3} = R^f_{1,2} + \frac{T^2_{1,2}R^f_{3,3}}{1 - R^f_{3,3}R^b_{2,1}} \tag{18}$$

$$R^b_{3,1} = R^b_{3,3} + \frac{T^2_{3,3}R^b_{2,1}}{1 - R^b_{2,1}R^f_{3,3}} \tag{19}$$

characteristics for individual layers of the ELFM need to be obtained before the optical property calculation for the complete system. Therefore, ray-tracing models for each layer were established in this section to calculate solar-optical characteristics of individual layers into the ELFM. Then optical properties of the whole glazing system were calculated based the recursion relations (Eq. (17) – (20)). Calculation results for optical properties of the whole ELFM, such as the light transmittance, front/back reflectance and absorptance were compared with that of the

$$A^f_{1,3} = \left(1 - T_{1,1} - R^f_{1,1}\right) + T_{1,1}R^f_{2,3}\left(1 - T_{1,1} - R^b_{1,1}\right) + \frac{T_{1,1}(1 - T_{2,2} - R^f_{2,2})}{1 - R^f_{2,3}R^b_{1,1}} + \frac{T_{1,2}R^f_{3,3}(1 - T_{2,2} - R^b_{2,2})}{1 - R^f_{2,3}R^b_{1,1}} + \frac{T_{1,2}(1 - T_{3,3} - R^f_{3,3})}{1 - R^f_{3,3}R^b_{2,1}} \tag{20}$$

where, $T_{i,j}$ is transmittance through glass layers i ($i = 1, 2, 3$) to j ($j = 1, 2, 3$). $R^f_{i,j}$ is front reflectance from glass layers i to j. $R^b_{j,i}$ is back reflectance from glass layers j to i. $A^f_{i,j}$ is front absorptance through glass layers i to j.

2.2.2. Method for acquiring optical properties

Based on the analysis in the last section, the solar-optical

CCPC-PV window model under different solar incident angles.

The ray-tracing model for the original CCPC-PV window (as described in our recent work by Li et al (2023) [46]) was separated into three layers. Then optical characteristics, such as the light transmittance, front/back reflectance and absorptance of three individual layers could be obtained from the separated simulation results. Some assumptions were made for the ray-tracing simulation of the individual

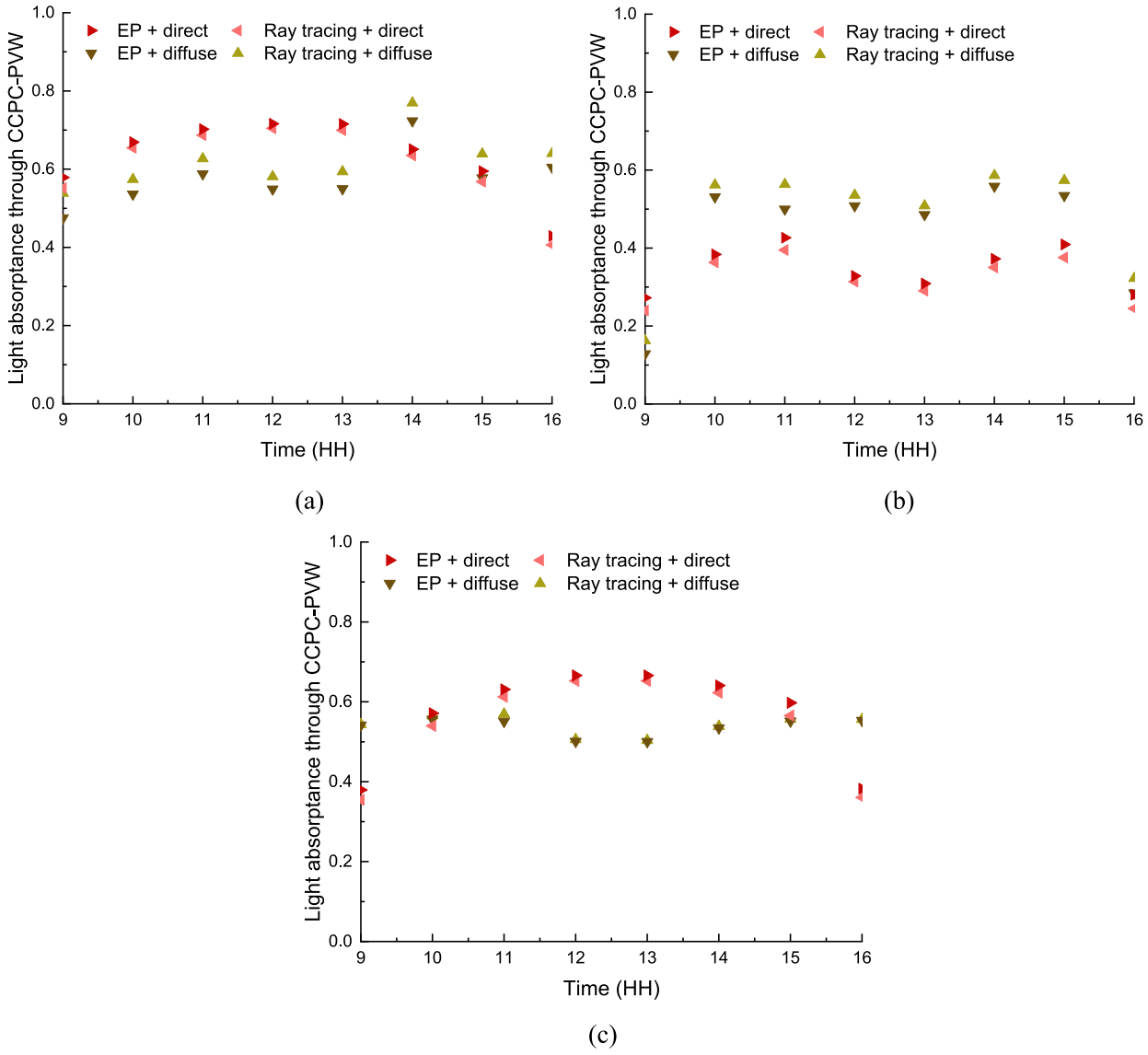

Fig. 14. Direct and diffuse solar absorptance on (a) 22nd Oct, (b) 22nd July, and (c) 22nd Mar.

layers into the ELFM. The heat released by the PV power generation was regarded as transmitted through the middle equivalent layer then absorbed by the indoor glass layer, which is consistent with the heat source distribution into the ELFM during the thermal modelling process (**Section 2.1.2**). Another assumption was based on the light behaviour difference between the multilayer glazing system with one-dimensional light transmission (Fig. 6 (a)) and ELFM with three-dimensional light transmission (Fig. 6 (b)). Rays' angles for reflected light and transmitted light are all the same as the incident angles (θ) for three layers into the multilayer glazing system (Fig. 6 (a)). When the air cavity contains a CCPC-PV structure, the light will be escaped from the bottom side surfaces of CCPC optics with different angles when the incident angle of the window outside surface is larger than the half acceptance angle. Therefore, the light incident on the indoor glass layer as shown in Fig. 6 (b) is from different directions. In this study, when the incident angle of the window outside surface is larger than 50°, optical properties of the third layer were all assumed as the value at 60° third layer incident angle based on the ray-tracing simulation for the leaking rays' direction. In addition, because of the complex light transmission through the CCPC-PV window, the back reflectance of three layers was all assumed as the same as the front reflectance.

The optical property of the complete ELFM under the direct solar radiation condition can be calculated using Eq. (6–17) – (6–20) based on the above ray-tracing simulation results for the individual layers. The solar radiation incident on the window outside surface consists of the direct solar radiation and diffuse solar radiation. The optical properties under diffuse solar radiation condition were obtained by regarding the diffuse solar radiation composed of direct solar radiation from all directions in the space, such as from 19 incident angles (−90° to 90° with 10° interval). Optical properties under diffuse solar radiation condition (η_{diff}), such as the diffuse transmittance, reflectance and absorption can be calculated from Eq. (21).

$$\eta_{diff} = \sum_{i=0}^{i=18} \frac{\eta_{dir}^{i}}{19} \times 100\% \tag{21}$$

where, η_{dir}^{i} is the transmittance, absorptance or reflectance under direct solar radiation condition at incident angle, *i*.

2.2.3. *Optical modelling under direct solar radiation condition*

Optical characteristics, including the light transmittance, reflectance and absorptance of individual layers into the ELFM at different incident angles (0° to 90° with 10° interval) and azimuth angles (90° to 270° with 15° interval) can be found in Appendix 1. Calculation results for the total

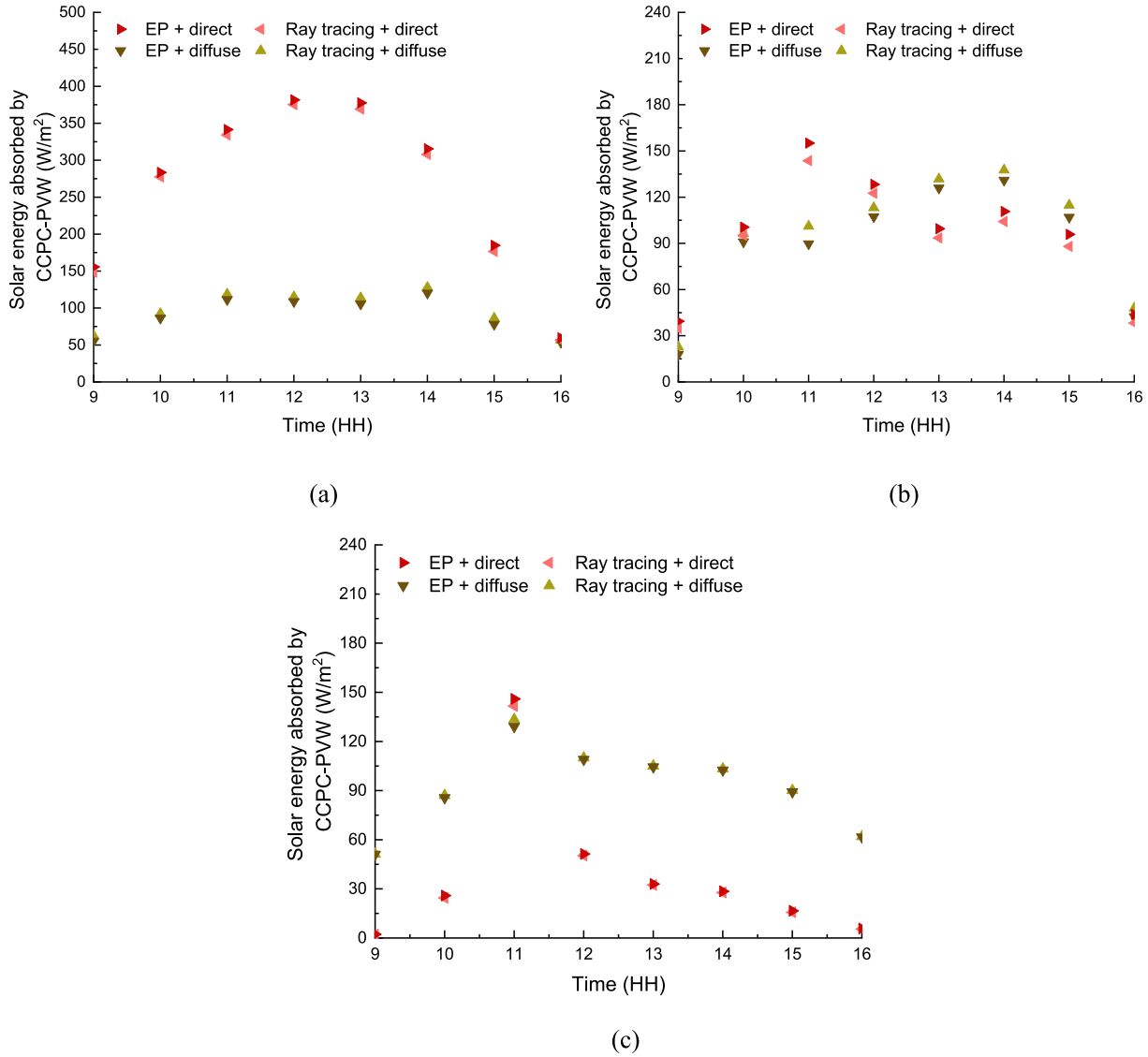

Fig. 15. Absorbed direct and diffuse solar radiation rate on (a) 22nd Oct, (b) 22nd July and (c) 22nd Mar.

transmittance, absorptance and reflectance of the ELFM at different incident angles and azimuth angles as shown in Fig. 7, were compared with that of the CCPC-PV window model. Deviations of the light transmittance, absorptance and reflectance between the ELFM and CCPC-PV window model at different solar positions were averaged as 1.97 %, 3.09 % and 5.68 %, which indicates that the proposed ELFM is relatively accurate to simulate the optical properties of the CCPC-PV window within EnergyPlus.

2.2.4. *Optical modelling under diffuse solar radiation condition*

Fig. 8 shows optical properties of the CCPC-PV window model and its ELFM under diffuse solar radiation condition. Maximum deviations of the diffuse transmittance, absorptance and reflectance for two models are all within 5 %.

2.3. *PV modelling algorithm for coupling into building performance simulation*

This section introduces electrical models used to predict the power generation of the PV system within EnergyPlus first. Then an electrical model based on the modifications of the one built in EnergyPlus has been established to estimate the power output of the CCPC-PV window.

2.3.1. *Electrical model in EnergyPlus*

There are three models used for predicting the PV power generation in EnergyPlus. The usable electrical power produced by 'Simple' model is calculated using Eq. (22).

$$P = A_{surf} \times f_{activ} \times G_{pv} \times \eta_{pv} \times \eta_{invert} \tag{22}$$

where, P is the electrical power produced by the PV array, W. A_{surf} is the net surface area. m^2. f_{activ} is the fraction of the surface area with active solar cells. G_{pv} is the solar radiation incident on the PV array, W/m^2. η_{pv} is the module conversion efficiency. η_{invert} is the DC to AC conversion efficiency.

2.3.2. *Method for acquiring the system output*

An electrical model was established based on the modification of above 'Simple' model to predict the power output of the CCPC-PV window. The PV efficiency is assumed as a fixed value for the 'Simple' model rather than changing with the PV temperature, which is unreasonable for most of PV systems especially for the concentrating PV. The relation between the PV efficiency (η_{pv}) and PV temperature (t_{pv}) can be calculated using Eq. (23). And the PV conversion efficiency at standard test condition (18)%) and temperature coefficient (0.0039/℃) were measured using spectrometer and solar simulator under indoor

conditions [46]. As mentioned in Section 2.1.4, the PV temperature can be substituted using the window inside surface temperature of the ELFM (Eq. (12)) as there is no PV temperature into the ELFM. Therefore, the relation between the PV efficiency and the window inside surface temperature of the ELFM can be calculated using Eq. (24).

$$\eta_{pv} = 0.18 \times \left(1 + 0.0039 \times \left(25 - t_{pv}\right)\right) \quad (23)$$

$$\eta_{pv} = 0.18 \times \left(1 + 0.0039 \times \left(23.77 - t_{si}\right)\right) \quad (24)$$

In addition to the PV conversion efficiency, the system output is also affected by the concentrating effect of the CCPC optics existing into the window. This concentrating effect can be represented by the ratio between the solar radiation (W/m^2) incident on PV surfaces into the CCPC-PV window, G_{cpv} and that of the flat one, G_{pv}. Fig. 9 shows the change of this concentrating ratio along with the incident angle (Fig. 9 (a)) and incident angle cosine value (Fig. 9 (b)) for solar rays from different azimuth angle (φ) ranges. For the incident angle smaller than 50°, the solar radiation incident on the PV surface into the CCPC-PV window is larger than that of the flat one because of the light concentrating effect. When the incident angle exceeds 50°, the solar radiation incident on the PV surface is less than that of the flat one because a large proportion of rays leaks from the bottom side surfaces of CCPC optics then enters into indoor space. Relations between this concentrating effect (G_{cpv}/G_{pv}) and incident angle cosine value ($\cos\theta$) were regressed as shown in Eq. (25) to Eq. (30) for different solar azimuth angle ranges.

$|\varphi\text{-}180^\circ| \le 7.5^\circ$

$$\frac{G_{cpv}}{G_{pv}} = -28.870(\cos\theta)^5 + 37.243(\cos\theta)^4 - 1.107(\cos\theta)^3 - 5.600(\cos\theta)^2 + 1.396\cos\theta - 0.010\left(R^2 = 0.992\right) \quad (25)$$

$7.5^\circ < |\varphi\text{-}180^\circ| \le 22.5^\circ$

$$\frac{G_{cpv}}{G_{pv}} = -52.163(\cos\theta)^5 + 88.668(\cos\theta)^4 - 40.410(\cos\theta)^3 + 6.277(\cos\theta)^2 + 0.331\cos\theta - 0.006\left(R^2 = 0.995\right) \quad (26)$$

$22.5^\circ < |\varphi\text{-}180^\circ| \le 37.5^\circ$

$$\frac{G_{cpv}}{G_{pv}} = 3.111(\cos\theta)^5 - 46.700(\cos\theta)^4 + 70.120(\cos\theta)^3 - 27.741(\cos\theta)^2 + 3.644\cos\theta - 0.004\left(R^2 = 0.995\right) \quad (27)$$

$37.5^\circ < |\varphi\text{-}180^\circ| \le 52.5^\circ$

$$\frac{G_{cpv}}{G_{pv}} = -75.322(\cos\theta)^4 + 102.35(\cos\theta)^3 - 36.496(\cos\theta)^2 + 4.325\cos\theta - 0.003\left(R^2 = 0.998\right) \quad (28)$$

$52.5^\circ < |\varphi\text{-}180^\circ| \le 67.5^\circ$

$$\frac{G_{cpv}}{G_{pv}} = -70.494(\cos\theta)^4 + 40.561(\cos\theta)^3 - 0.201(\cos\theta)^2 - 0.125\cos\theta\left(R^2 = 1\right) \quad (29)$$

$67.5^\circ < |\varphi\text{-}180^\circ| \le 90.0^\circ$

$$\frac{G_{cpv}}{G_{pv}} = -14.808(\cos\theta)^2 + 4.337\cos\theta\left(R^2 = 1\right) \quad (30)$$

After considering above two modifications based on the 'Simple' model within EnergyPlus, the power output of the CCPC-PV window (Q_e) can be calculated using Eq. (31).

$$Q_e = P \times G_{cpv}/G_{pv} \times \left(1 + 0.0039 \times \left(23.77 - t_{si}\right)\right) \quad (31)$$

2.4. Integrating the CCPC-PV window model into building simulation software

In this section, detailed methods for coupling the thermal, optical, and electrical properties mentioned above into the energy performance simulation for a building window are presented based on an office room established in EnergyPlus.

2.4.1. Weather data

This study was performed over one hour time step using the IWEC (International Weather for Energy Calculation) weather file for London (latitude 51.5°N and the longitude 0°W). Fig. 10 (a) shows the total solar radiation (direct + diffuse) incident on window outside surface on 22nd of every month and those with larger value (more than 2 kWh/m^2) were initially chosen as the representative weather data. As illustrated in Section 2.2, the light transmission under the direct solar radiation condition is different from that of the diffuse solar radiation condition.

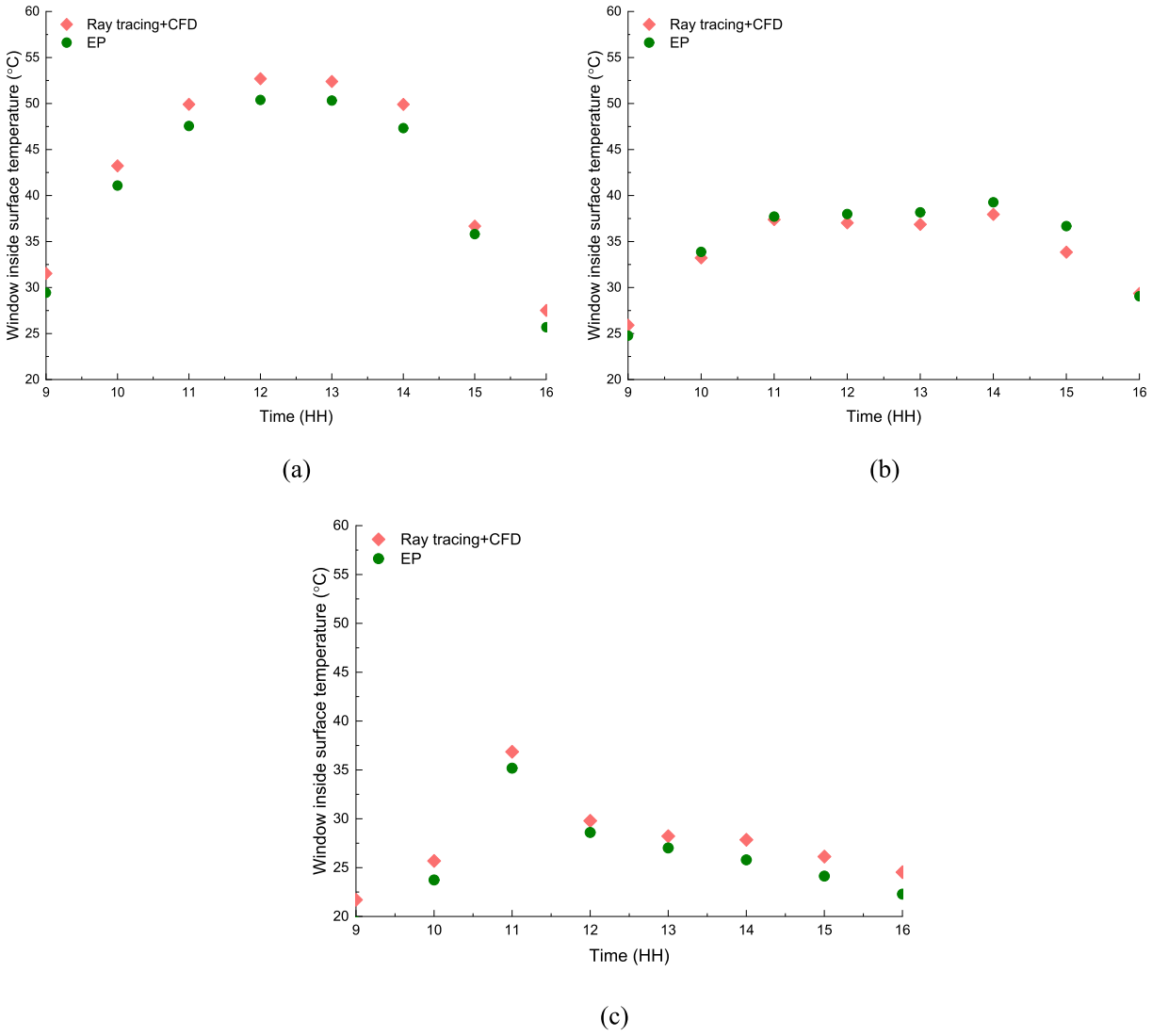

Fig. 16. Window inside surface temperature on (a) 22nd Oct, (b) 22nd July, and (c) 22nd Mar.

Therefore, the chosen weather data should include different solar radiation conditions. Fig. 10 (b) shows the proportion of the direct solar radiation on the total solar radiation incident on the window outside surface. In this study, the weather data on 22nd Mar (25 % direct + 75 % diffuse), 22nd July (53 % direct + 47 % diffuse), and 22nd Oct (71 % direct + 29 % diffuse) was selected as representative solar radiation conditions to conduct the performance simulation for a building window. Fig. 11 shows the weather data, such as the air temperature, solar incident angle, solar azimuth angle and solar radiation incident on the window outside surface on 22nd Oct, 22nd July, and 22nd Mar in London.

2.4.2. Simulation setup

For this section, a simple office-building model was established to simulate the thermal and energy performance of the CCPC-PV window in a building under specific conditions. The office is south facing and considered as part of a large building. The boundary condition of the south wall of the office room was set as 'exposed to the outdoor environment' and the U-value of the exterior south wall was assumed as 0.26 $W/m^2 \cdot K$ based on the maximum allowed building elements U-values in the latest UK building regulations [50]. While those of rest walls and floor were set to be adiabatic (i.e., no heat gains and losses through them) [26]. The office has dimensions of 3 m (width) × 3 m (length) × 3 m (height), and a window with dimensions of 0.6 m (height) × 0.6 m (width) is on the south exterior wall with a sill level of 1.1 m above the ground. The HVAC was assumed to be a unitary system with direct expansion cooling and gas heating and a single set point temperature of 24 °C (NFRC) is used all year round. The inside and outside surface convective heat transfer coefficients were fixed as 3.6 $W/m^2 \bullet K$ [44] and 8 $W/m^2 \bullet K$ [51] and the emissivity of window surfaces was set as 0.84. As this study focused on the method to integrate the CCPC-PV window into a building simulation model, equipment and lighting loads were all not considered in this model.

2.4.3. Coupling above thermal, optical, and electrical properties into building performance simulation

To couple the thermal properties of the CCPC-PV window into building performance simulation, the ELFM was used and the thermal conductivities of two equivalent layers (K_{e1} and K_{e2}) and the indoor glass layer (K_g) as shown in Table 1 were input into the glazing material property within EnergyPlus to conduct the window heat transfer calculation. To couple the solar-optical properties of the CCPC-PV window into building performance simulations, the optical data for individual layers into the ELFM under different incident angles (Appendix 1) was input into optical data tables within EnergyPlus. Then the 'Energy Management System (EMS)' function within EnergyPlus was employed

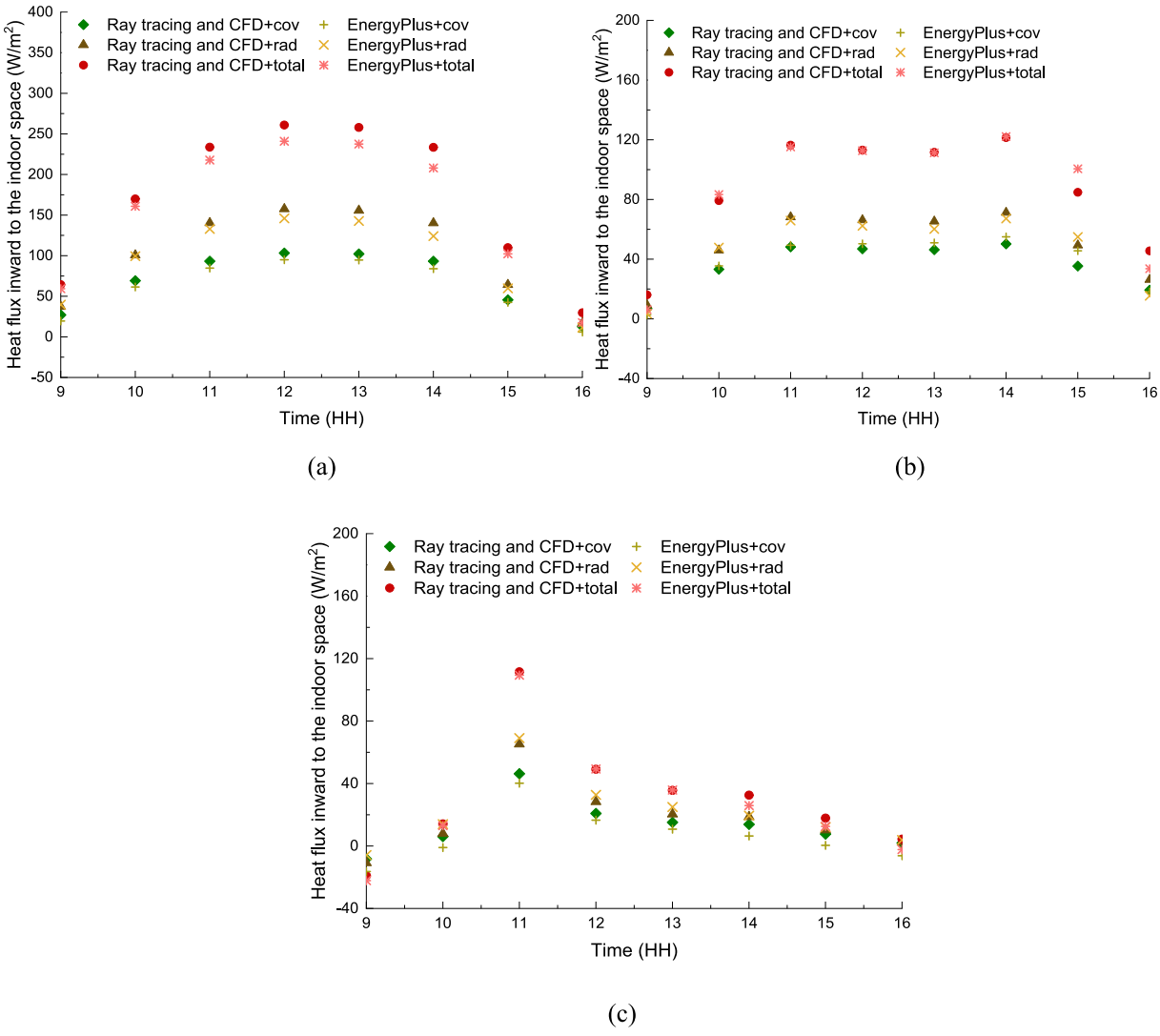

Fig. 17. Heat flux inward to the indoor space on (a) 22nd Oct, (b) 22nd July and (c) 22nd Mar.

to couple these optical tables for solar rays from different azimuth angle ranges. In addition, PV modelling algorithms as described in Eq. (23) – (31) were also inserted into the 'EMS' function to predict the on-site power generation.

3. Results and discussion

In this section, the solar-optical properties (light transmittance and absorptance) of the ELFM representing the CCPC-PV window within EnergyPlus are discussed first. Then the SHGC and power output of the ELFM are presented on three days with different solar radiation conditions. The simulation results of the ELFM within EnergyPlus are all compared with the results from CFD combined ray-tracing method for the original CCPC-PV window.

3.1. Light transmittance

This section presents the light transmittance of the ELFM on 22nd Oct, 22nd July, and 22nd Mar within EnergyPlus. Fig. 12 shows that the direct and diffuse light transmittance of the ELFM on 22nd Mar, 22nd July, and 22nd Oct within EnergyPlus are in good agreement with ray-tracing simulation results for the original CCPC-PV window. Peak values for the light transmittance under direct solar radiation condition occur at early morning or afternoon on 22nd Oct and 22nd Mar and it occurs at around noon on 22nd July when incident angles are all around 60°. In addition, the diffuse solar transmittance of the ELFM always has the highest values at around noon. This is because the diffuse transmittance is highest when the azimuth angle is around 180° (Fig. 8).

Fig. 13 shows the transmitted direct, diffuse, and total solar radiation on 22nd Mar, 22nd July and 22nd Oct. Even though the direct solar radiation accounts for 71 % of the total solar radiation incident on window outside surface on 22nd Oct (Fig. 10 (b)), the transmitted direct solar radiation is near the same as that of the diffuse solar radiation (Fig. 13 (a)). This is because the direct light transmittance is lower than that of the diffuse light transmittance at most of the daytime (Fig. 12 (a)). Even though the amount of the direct solar radiation is close to that of the diffuse solar radiation on 22nd July, the transmitted direct solar radiation is larger than that of the diffuse solar radiation. This is because the direct solar transmittance is higher than the diffuse solar transmittance on 22nd July. The transmitted diffuse solar energy is larger than of the direct solar radiation on 22nd Mar because the diffuse solar radiation accounts for 75 % of the total solar radiation incident on window outside surface. The total transmitted (direct and diffuse) solar radiation was calculated as 661.01 Wh/m^2, 979.10 Wh/m^2 and 363.02 Wh/m^2 on 22nd Oct, 22nd July, and 22nd Mar, respectively. The corresponding data for ray-tracing simulation is 649.51 Wh/m^2, 977.98 Wh/m^2 and 356.15 Wh/m^2. The deviation was calculated as 1.77 %, 0.12 % and 1.93 % on 22nd Oct, 22nd July, and 22nd Mar, respectively.

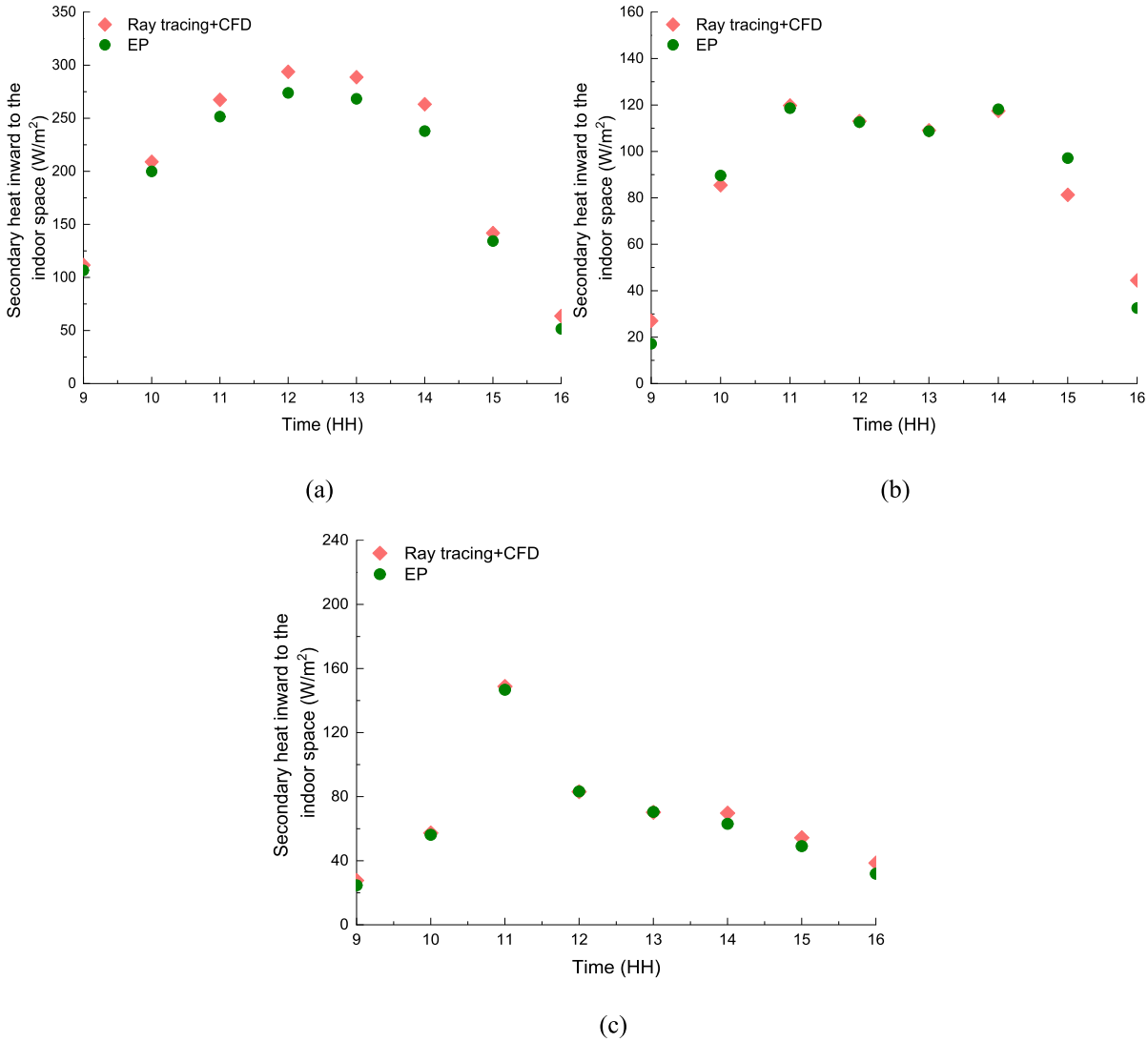

Fig. 18. Secondary heat flux inward to the indoor space on (a) 22nd Oct, (b) 22nd July and (c) 22nd Mar.

3.2. Light absorptance

The light transmittance as described in the last section is a part of the SHGC value for a building window. In addition to the light transmittance, the SHGC is also determined by the amount of solar energy absorbed then released to the indoor space through convective and radiative heat transfer. Fig. 14 shows simulation results for the light absorptance of the ELFM on 22nd Oct, 22nd July, and 22nd Mar within EnergyPlus and the results are also compared with ray-tracing results for the original CCPC-PV window. The solar absorptance under direct solar radiation condition increases first at around noon then gradually decreases on 22nd Oct and 22nd Mar. This is because the solar absorptance on these two days is mainly affected by the incident angle and the solar absorptance is larger for a smaller incident angle at noon. However, this change is different on 22nd July. This is because the incident angle on 22nd July is larger than that for the other two days and the solar absorptance is affected by both incident angle and azimuth angle. In addition, the solar absorptance under diffuse solar radiation condition changes between 0.5 and 0.6 at most of the daytime on three days. The total absorbed (direct + diffuse) solar energy rate is shown in Fig. 15. The deviation of the absorbed solar energy rate using two methods was calculated as around 0 % on three days. Based on the discussion in **Section 3.1** and **Section 3.2**, the proposed ELFM is relatively accurate to represent the CCPC-PV window in terms of its solar-optical properties.

3.3. Secondary heat

The amount of solar energy absorbed by the CCPC-PV window as described in the last section will ultimately affect window thermal and energy performances. In this section, simulation results for the window inside surface temperature and the heat flux absorbed by the window then subsequently conducted, convected, and radiated to the interior of the building (secondary heat) [25,52] are discussed on 22nd Oct, 22nd July, and 22nd Mar within EnergyPlus. The simulated results are also compared with those calculated using 3D CFD combined ray-tracing method for original CCPC-PV window. As shown in Fig. 16, the window inside surface temperature increases first from 9am to around noon then decreases until 16 pm on 22nd Oct, 22nd July, and 22nd Mar. This is because the outdoor air temperature and total absorbed solar energy all increase from 9am to around noon first then decrease until 16 pm. The deviation of the window inside surface temperature using two methods was averaged as 4.73 %, 2.18 % and 5.80 % on 22nd Oct, 22nd July, and 22nd Mar, respectively.

Fig. 17 shows the convective and radiative heat flux inward to the indoor space on 22nd Oct, 22nd July, and 22nd Mar within EnergyPlus. The total convective heat flux was calculated as 488.17 Wh/m^2, 307.82 Wh/m^2 and 51.19 Wh/m^2 on 22nd Oct, 22nd July, and 22nd Mar, respectively. The corresponding data for the 3D CFD combined ray-tracing method is 546.72 Wh/m^2, 286.54 Wh/m^2 and 103.72 Wh/m^2.

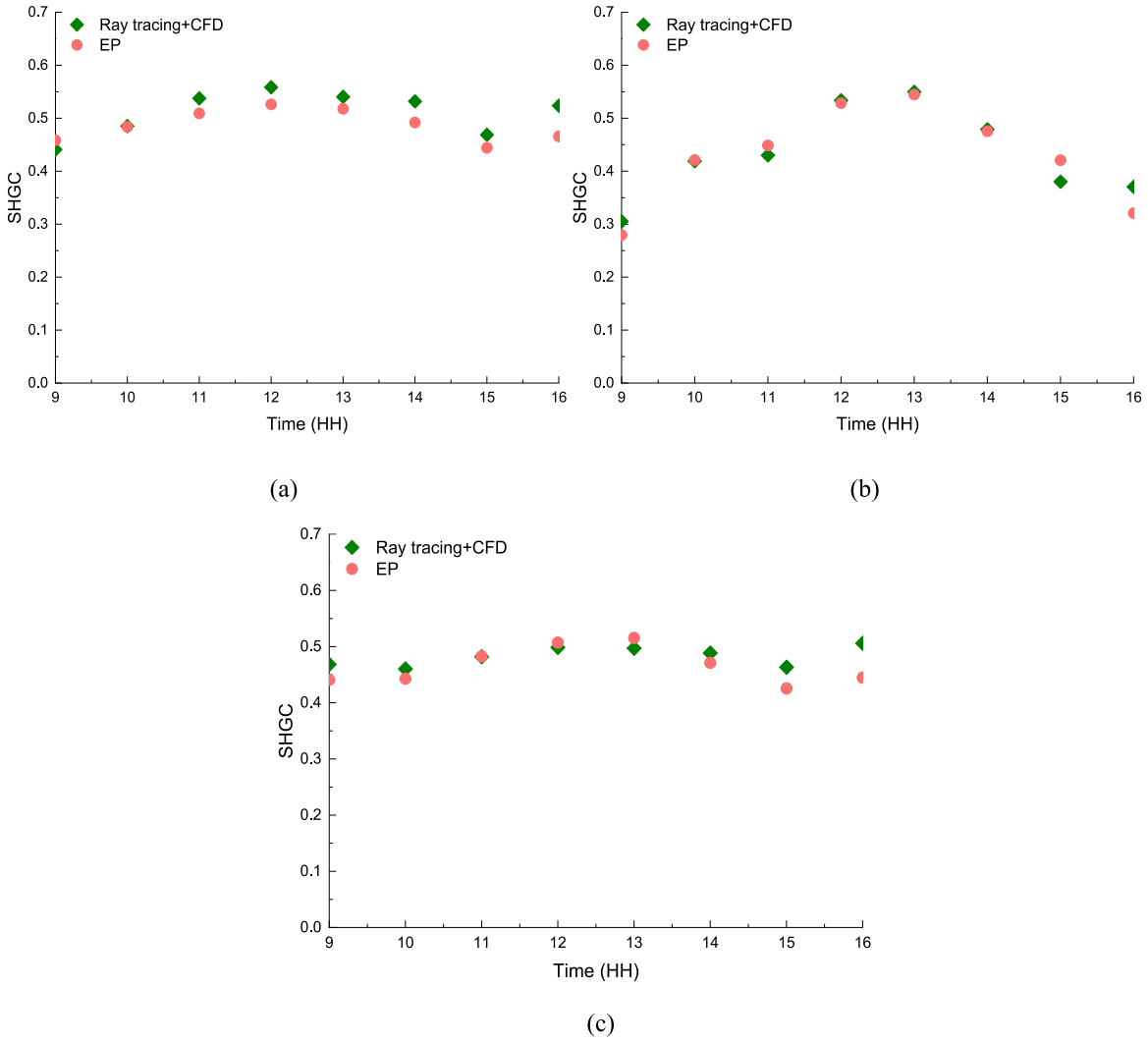

Fig. 19. SHGC results on (a) 22nd Oct, (b) 22nd July and (c) 22nd Mar.

The difference for using two methods accounts for 1.32 %, 0.57 % and 5.54 % of the total solar radiation incident on the window outside surface. The total radiative heat flux was simulated as 756.50 Wh/m^2, 377.38 Wh/m^2 and 170.62 Wh/m^2 on 22nd Oct, 22nd July, and 22nd Mar within EnergyPlus. The corresponding data for the 3D CFD combined ray-tracing method is 813.23 Wh/m^2, 401.90 Wh/m^2 and 142.73 Wh/m^2. The difference for using two methods accounts for 1.28 %, 0.66 % and 1.49 % of the total solar radiation incident on the window outside surface. The deviation of the total heat flux including the convection and radiation based on two methods was calculated as 2.61 %, 0.09 % and 1.32 % on 22nd Oct, 22nd July, and 22nd Mar, respectively.

Fig. 18 shows the secondary heat inward to the indoor space on three days. It was simulated as 1524.04 Wh/m^2, 694.48 Wh/m^2 and 525.37 Wh/m^2 on 22nd Oct, 22nd July, and 22nd Mar within EnergyPlus. The corresponding data for the 3D CFD combined ray-tracing method is 1639.33 Wh/m^2, 697.70 Wh/m^2 and 550.01 Wh/m^2. The difference of the secondary heat using two methods accounts for 2.61 %, 0.09 % and 1.32 % of the total solar radiation incident on window outside surface. Based on above analysis, the proposed ELFM is accurate to represent the CCPC-PV window to be coupled into the building performance simulation.

3.4. SHGC

The SHGC represents a crucial indicator of window properties that influences the thermal and energy performance of buildings [53]. It consists of the fraction of external solar radiation that directly transmitted and absorbed then released inward (secondary heat as described in the last section). The direct transmitted part including the transmitted direct and diffuse solar radiation is presented in **Section 3.1** while the secondary inward heat is presented in **Section 3.3**. Fig. 19 shows the calculated SHGC of the ELFM on three days within EnergyPlus and it is also compared with the results from 3D CFD combined ray-tracing method for the original CCPC-PV window. Fig. 20 shows the total transmitted solar energy including the transmitted direct and diffuse solar radiation as well as the secondary heat inward to the indoor space. The total transmitted solar energy was calculated as 2185.05 Wh/m^2, 1673.58 Wh/m^2 and 888.39 Wh/m^2 on 22nd Oct, 22nd July, and 22nd Mar, respectively. The corresponding data for the 3D CFD combined ray-tracing method is 2288.84 Wh/m^2, 1675.68 Wh/m^2 and 906.17 Wh/m^2. The deviation was calculated as 2.35 %, 0.07 % and 0.95 % on 22nd Oct, 22nd July, and 22nd Mar, respectively.

Fig. 21 shows the SHGC regression results based on the above simulation results on 22nd Oct, 22nd July, and 22nd Mar within EnergyPlus and the regression was also conducted based on the results from 3D CFD combined ray-tracing method. As X-axis represents the total solar radiation incident on window outside surface while Y-axis represents the total transmitted solar energy, the slope of the regressed equation represents the SHGC value of the CCPC-PV window. Therefore, the SHGC was regressed as 0.486 based on the simulation result within

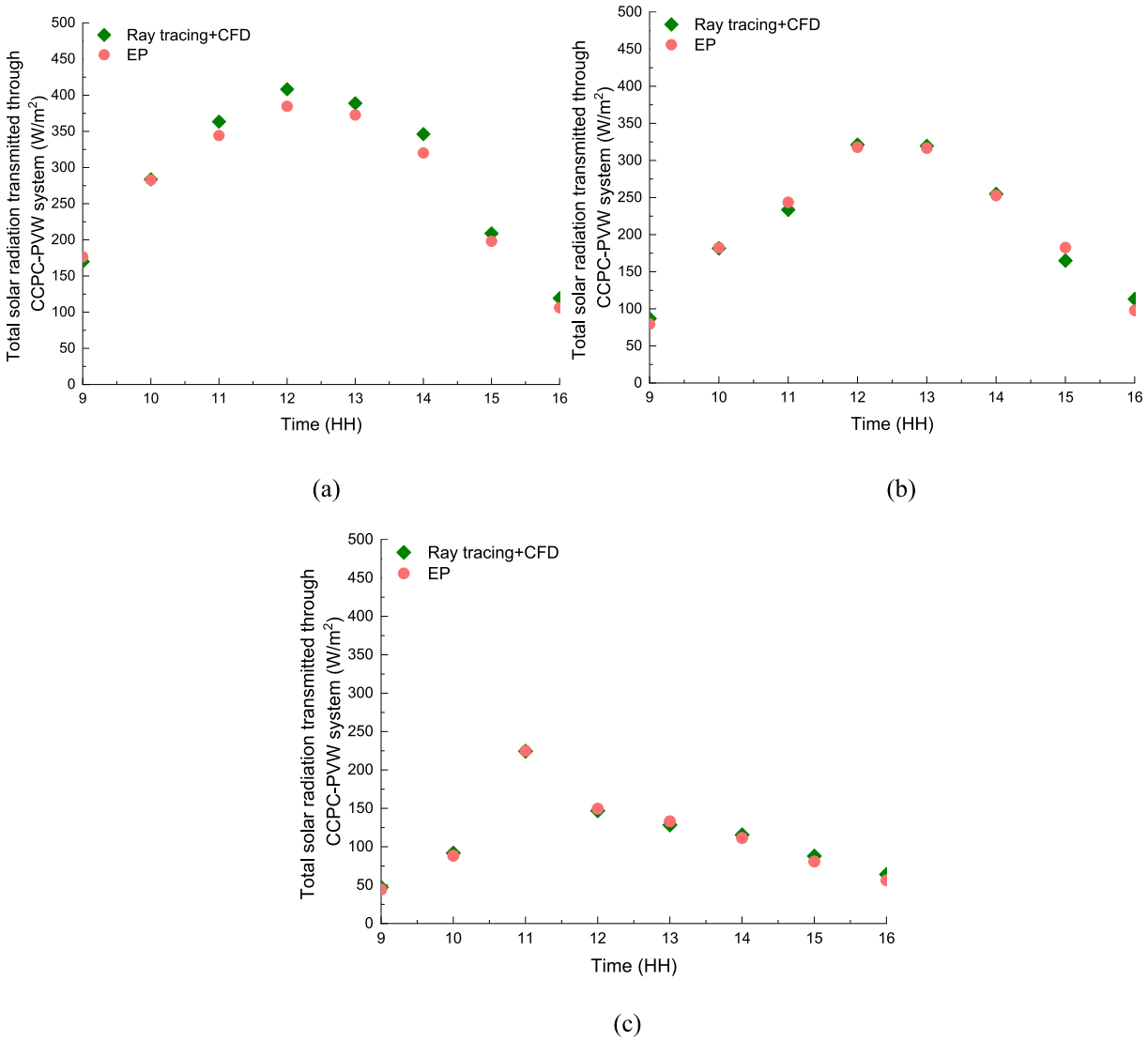

Fig. 20. Total transmitted solar energy rate on (a) 22nd Oct, (b) 22nd July and (c) 22nd Mar.

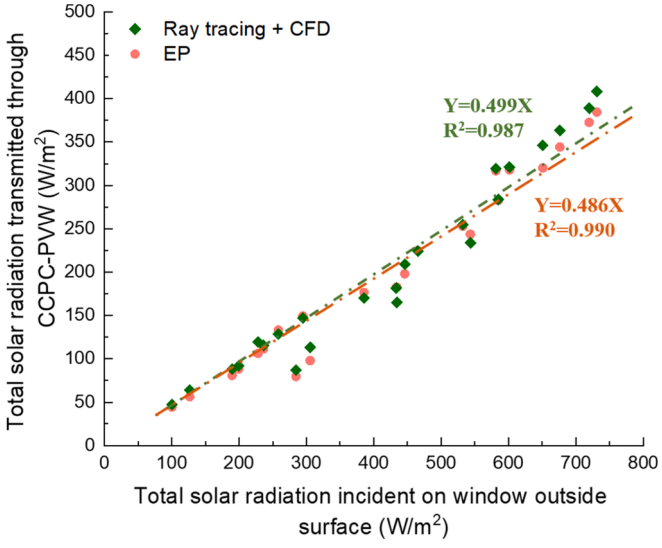

Fig. 21. SHGC regression based on the EnergyPlus simulation and 3D CFD combined ray-tracing simulation.

EnergyPlus and 0.499 based on the results from 3D CFD combined ray-tracing method for the original CCPC-PV window with a 2.68 % deviation.

3.5. *Electricity generation*

Fig. 22 shows the power output of the ELFM on 22nd Oct, 22nd July, and 22nd Mar within EnergyPlus. The total electricity generation was predicted as 690.71 Wh/m^2 on three days within EnergyPlus. And the corresponding data for 3D CFD combined ray-tracing method is 685.39 Wh/m^2 within 1 % deviation.

3.6. *Summary*

Table 5 summarises the solar-optical, thermal, and electrical performance of the CCPC-PV window on three specific days representing different solar radiation conditions in London. The simulation results from EnergyPlus are then compared to the results obtained from a validated CFD combined ray-tracing method for the original CCPC-PV window. It can be observed that the deviations in various parameters between the two methods are all within 5 %. This suggests that the proposed method for integrating the complex CCPC-PV window into building simulation software is relatively accurate for characterising

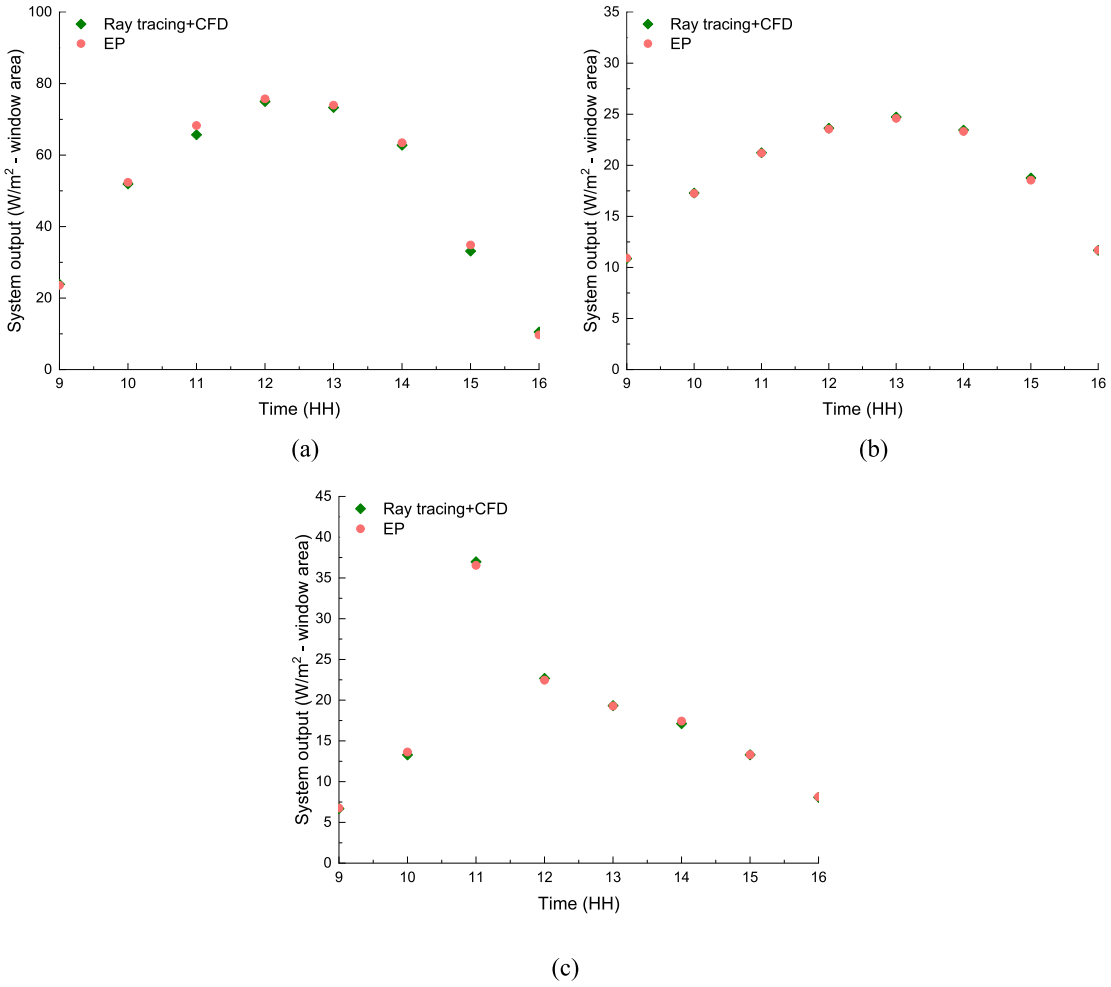

Fig. 22. Electricity generation on (a) 22nd Oct, (b) 22nd July and (c) 22nd Mar.

Table 5
Performance comparison of CCPC-PV window using EnergyPlus and a validated CFD combined ray-tracing method over three days (22nd Oct, 22nd July and 22nd Mar) representing different solar radiation conditions in London.

Window performance	Parameters	Results from EnergyPlus*	Results from CFD combined ray-tracing*	Deviation
Solar-optical	Total transmitted solar radiation (Wh/m^2)	2003.13	1983.64	0.98 %
	Total absorbed solar radiation (Wh/m^2)	5348.22	5348.22	0.00 %
Thermal	Total secondary heat (Wh/m^2)	2743.89	2887.04	4.96 %
	SHGC (−)	0.486	0.499	2.68 %
Electrical	Total electricity generation (Wh/m^2)	690.71	685.39	0.78 %

*The table data is summarised over three days.

building performance when this window is installed.

4. Case study – annual building performance simulation with CCPC-PV window

The previous results show that the proposed comprehensive method accurately integrates the thermal, optical, and electrical properties of the CCPC-PV window into EnergyPlus. In this section, a case study was conducted to investigate the overall energy performance of a small cellular office room using the CCPC-PV window, based on the aforementioned window integration method. The numerical model, as discussed in Section 2.4.2, was also employed in this section. The analysis of the numerical model was conducted under three Window-to-Wall Ratios (WWRs), representing typical small, medium, and large window sizes installed on a building's south wall [40], as illustrated in Fig. 23. The energy performance of the office room integrated with the CCPC-PV window was also compared with that of a similarly structured double-glazed system.

4.1. Weather data

The case study in this section was also conducted based on the climate conditions in London (latitude 51.5°N and the longitude 0°W). The IWEC (International Weather for Energy Calculation) weather file for this city with one-hour time step data was used to conduct the annual building performance simulation. Fig. 24 shows the monthly average diurnal variations in air temperature, direct and diffuse solar radiation, and the solar incident angle on a south-facing window in London.

4.2. Additional simulation setup

Based on the cellular office room model in **Section 2.4.2**, additional simulation setups were incorporated for building performance simulation assuming the installation of the CCPC-PV window on its south

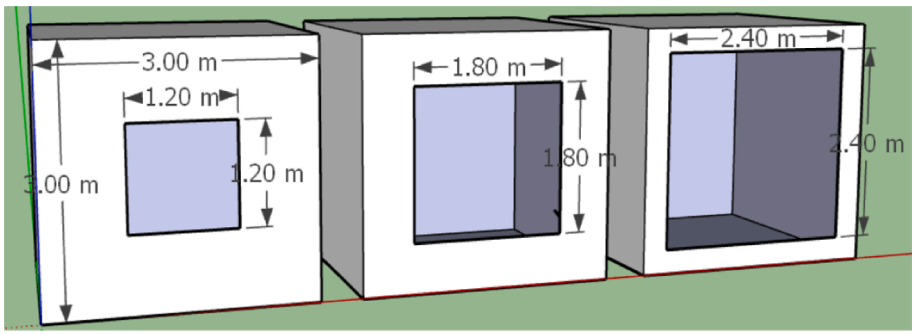

Fig. 23. Diagrams of the office room using a Window-to-Wall Ratio (WWR) of (a) 16%, (b) 36%, and (c) 64%.

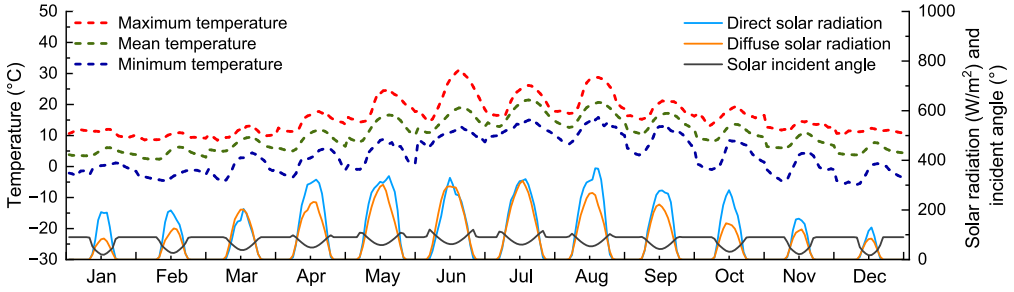

Fig. 24. Monthly average diurnal variations in air temperature, solar radiation, and solar incident angle on a south-facing window in London.

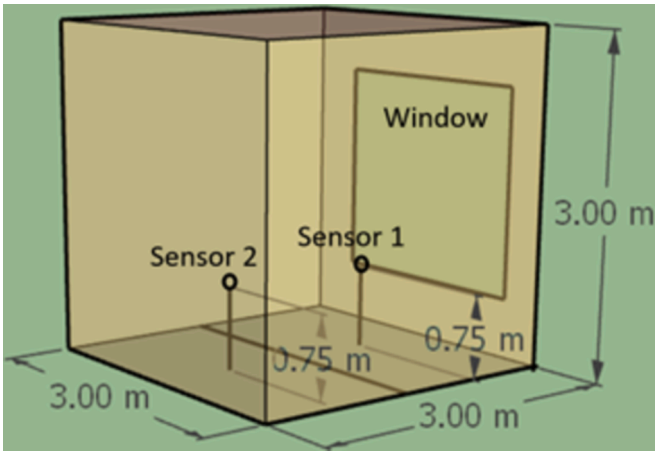

Fig. 25. Daylight sensor deployment in the office room.

façade. The occupancy hour was assumed to be from 9:00 to 17:00 on weekdays for one person in the room all year around. The equipment and lighting loads, which were only counted during working hours, were assumed to be 15 W/m^2 and 9 W/m^2 [26,54], respectively. The electric lighting was set to be automatically controlled by two zoned daylight sensors at the centre of each zone with a 0.75 m height above the floor as shown in Fig. 25. Sensor 1 is in zone 1 close to the window (0.75 m away) while sensor 2 is in zone 2 further away from the window (2.25 m away). The artificial lighting was switched on when the daylight illuminance detected by these two sensors fell below 500 lx [27,54]. Shading and glare control were not considered in this study. A unitary HVAC system with direct expansion cooling and gas heating was used to maintain the indoor air temperature at 21 °C in winter and 24 °C in summer based on CIBSE guide A [54] during working hours all year round.

4.3. Annual energy performance of a building with CCPC-PV window

Fig. 26 shows the predicted annual energy consumption and power generation of the office room with respect to different WWRs. As the WWR increases from 16 % to 64 %, more sunlight can penetrate the indoor space, contributing to reduced lighting energy consumption but increased cooling energy consumption. Meanwhile, there is a slight increase in heating energy consumption because the heat loss, due to the indoor and outdoor air temperature difference, exceeds the solar heat gain as the window area is enlarged. As a result, the annual total energy consumption of the office room using the CCPC-PV window rises as the WWR increases from 16 % to 64 %. In addition, the office room utilising the CCPC-PV window consumes more total energy when compared to a similarly structured double-glazed window under all WWR applications. However, the CCPC-PV window can produce additional power and the annual power generation significantly increases with the enlargement of the window area. Table 6 summarises the annual net energy consumption and energy-saving potential for the office room using windows with different WWRs. As the WWR increases from 16 % to 64 %, the net energy consumption decreases from 29.28 kWh/m^2 to 21.87 kWh/m^2 for the office room using the CCPC-PV window. Meanwhile, the energy-saving percentage increases from 13.66 % to 56.86 % when compared to a similarly structured double-glazed window. These results indicate that the CCPC-PV window is more suitable for installation with a larger window area, such as a 64 % WWR application.

5. Conclusions

This research has developed a comprehensive workflow to couple the thermal, optical, and electrical properties of the complex PV window system into the building simulation software. An Equivalent Layer Fenestration Model (ELFM), representing the CCPC-PV window, to be coupled into the building performance simulation within EnergyPlus was proposed. The thermal model based on a validated 3D CFD combined ray-tracing method, optical model based on the validated

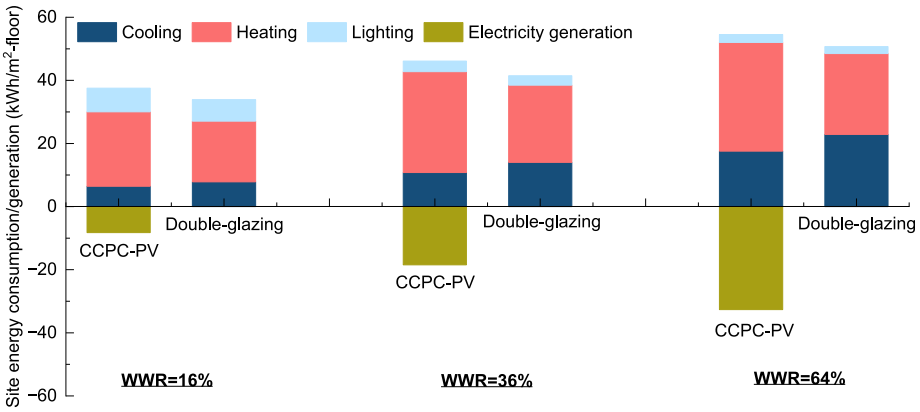

Fig. 26. Annual energy consumption and generation for the office room using CCPC-PV window and double-glazing for various WWRs' application under London climate condition.

Table 6
Annual net energy consumption (kWh/m^2 -floor) for different WWRs (Values in brackets are net energy savings relative to the double-glazed window) in London.

	WWR = 16 %	WWR = 36 %	WWR = 64 %
CCPC-PV window	29.28 (13.66 %)	27.66 (33.30 %)	21.87 (56.86 %)
Double-glazed window	33.92	41.46	50.70

recursion algorithm combined ray-tracing method and electrical model based on modifications of the 'Simple' model within EnergyPlus through experimental measurement were established to investigate the thermal, optical, and electrical properties of the ELFM. Then the above properties were all coupled into the building simulation model within EnergyPlus, and a case study was conducted to investigate the annual energy performance of an office room using the CCPC-PV window. The conclusions can be drawn as follows:

(1) The equivalent layer fenestration model was proved to accurately incorporate the thermal, solar-optical, and electrical properties of the complex CCPC-PV window into the energy performance simulation for a building window within EnergyPlus.
(2) The deviation of the total transmitted (directly transmitted + secondary heat) solar energy between the ELFM and original CCPC-PV window model is less than 3 % on three days representing different solar radiation conditions in London.
(3) The SHGC was regressed as 0.486 based on EnergyPlus simulation results, which has a 2.7 % deviation from the value obtained based on 3D CFD combined ray-tracing results for the original CCPC-PV window (0.499).
(4) The total power output of the ELFM on 22nd Oct, 22nd July, and 22nd Mar within EnergyPlus was predicted as 690.71 Wh/m^2, which has a 0.78 % deviation from the data based on 3D CFD combined ray-tracing method for the original CCPC-PV window (685.39 Wh/m^2).
(5) The CCPC-PV window is more suitable for a larger WWR application (e.g., 64 %), which achieves a 56.86 % energy-saving percentage when compared to a similarly structured double-glazed window under London climate conditions.

This study has focused on the method of integrating a complex fenestration system into the building energy performance simulation within existing simulation software. The results demonstrate that the proposed equivalent layer fenestration model, which can be coupled with EnergyPlus, accurately represents the CCPC-PV window in terms of its thermal, optical, and electrical properties. Additionally, a simple case study was conducted to initially assess the energy-saving potential of the CCPC-PV window when compared to a similarly structured double-glazed window. Future investigations will provide a detailed energy and daylight performance prediction of buildings using the CCPC-PV window under various climate conditions.

CRediT authorship contribution statement

Xue Li: Writing – original draft, Validation, Software, Methodology, Investigation, Formal analysis, Conceptualization. **Yanyi Sun:** Writing – review & editing, Supervision, Methodology, Conceptualization. **Yupeng Wu:** Writing – review & editing, Supervision, Methodology, Funding acquisition, Conceptualization.

Declaration of competing interest

The authors declare that they have no known competing financial interests or personal relationships that could have appeared to influence the work reported in this paper.

Acknowledgments

This work was supported by a joint PhD studentship awarded to Xue Li by the Faculty of Engineering, University of Nottingham, UK, and the China Scholarship Council, China. This work was also supported by the Engineering and Physical Sciences Research Council, UK [grant number EP/S030786/1].

Appendix 1. Optical characteristics of individual layers in the ELFM

.

Table A1-1
. Optical characteristics of individual layers into the ELFM representing the CCPC-PV window.

(a) For rays from 172.5° to 187.5° azimuth angles

Incident angle (°)	Front reflectance (%)			Transmittance (%)			Back reflectance (%)		
	1st *	2nd *	3rd *	1st	2nd	3rd	1st	2nd	3rd
0	4.31	0.75	13.80	90.21	96.45	15.12	4.31	0.75	13.80
10	4.32	0.74	13.82	90.16	96.00	14.82	4.32	0.74	13.82
20	4.33	0.79	13.88	90.05	95.48	14.13	4.33	0.79	13.88
30	4.45	0.84	14.78	89.76	94.85	13.76	4.45	0.84	14.78
40	4.90	3.75	14.41	89.09	90.11	19.57	4.90	3.75	14.41
50	6.06	7.50	16.59	87.73	85.02	49.23	6.06	7.50	16.59
60	9.26	5.94	16.45	84.44	84.62	66.18	9.26	5.94	16.45
70	17.75	7.07	16.47	76.28	84.88	72.84	17.75	7.07	16.47
80	39.30	4.84	16.39	56.16	87.79	76.69	39.30	4.84	16.39
90	100.00	100.00	100.00	0.00	0.00	0.00	100.00	100.00	100.00

(b) For rays from 157.5°-172.5°& 187.5°-202.5° azimuth angles

Incident angle (°)	Front reflectance (%)			Transmittance (%)			Back reflectance (%)		
	1st *	2nd *	3rd *	1st	2nd	3rd	1st	2nd	3rd
15	4.32	0.75	13.86	90.11	95.84	14.40	4.32	0.75	13.86
20	4.34	1.03	13.91	90.04	94.98	13.79	4.34	1.03	13.91
30	4.46	2.17	14.82	89.75	92.81	13.28	4.46	2.17	14.82
40	4.91	5.72	14.60	89.07	87.51	17.39	4.91	5.72	14.60
50	5.99	10.70	16.35	87.79	80.57	44.75	5.99	10.70	23.42
60	9.32	7.87	16.57	84.37	82.01	64.93	9.32	7.87	16.57
70	17.36	7.36	16.60	76.65	83.49	72.20	17.36	7.36	16.60
80	40.67	7.15	16.52	54.89	82.80	76.47	40.67	7.15	16.52
90	100.00	100.00	100.00	0.00	0.00	0.00	100.00	100.00	100.00

(c) For rays from 142.5°-157.5° & 202.5°-217.5° azimuth angles

Incident angle (°)	Front reflectance (%)			Transmittance (%)			Back reflectance (%)		
	1st *	2nd *	3rd *	1st	2nd	3rd	1st	2nd	3rd
30	4.45	0.84	14.78	89.76	94.85	13.76	4.45	0.84	14.78
40	4.89	7.34	16.09	89.10	84.28	14.95	4.89	7.34	16.09
50	6.05	15.29	20.71	87.74	73.88	20.29	6.05	15.29	20.71
60	9.41	15.04	16.62	84.29	71.90	59.67	9.41	15.04	16.62
70	17.91	9.87	16.63	76.13	77.86	71.52	17.91	9.87	16.63
80	38.02	7.52	16.54	57.35	81.08	76.15	38.02	7.52	16.54
90	100.00	100.00	100.00	0.00	0.00	0.00	100.00	100.00	100.00

(d) For rays from 127.5°-142.5° & 217.5°-232.5° azimuth angles

Incident angle (°)	Front reflectance (%)			Transmittance (%)			Back reflectance (%)		
	1st *	2nd *	3rd *	1st	2nd	3rd	1st	2nd	3rd
45	5.30	7.20	16.74	88.59	85.90	28.92	5.30	7.20	16.74
50	6.05	16.17	26.69	87.73	72.91	11.36	6.05	16.17	26.69
60	9.22	23.99	37.09	84.47	61.08	21.59	9.22	23.99	37.09
70	17.46	16.83	27.22	76.55	68.21	58.00	17.46	16.83	27.22
80	39.66	9.77	16.35	55.82	78.28	75.77	39.66	9.77	16.35
90	100.00	100.00	100.00	0.00	0.00	0.00	100.00	100.00	100.00

(e) For rays from 112.5°-127.5° & 232.5°-247.5° azimuth angles

Incident angle (°)	Front reflectance (%)			Transmittance (%)			Back reflectance (%)		
	1st *	2nd *	3rd *	1st	2nd	3rd	1st	2nd	3rd
60	9.26	5.94	16.45	84.44	84.62	66.18	9.26	5.94	16.45
70	17.57	26.27	42.48	76.44	52.80	26.59	17.57	26.27	42.48
80	39.70	15.50	16.44	55.79	71.55	74.34	39.70	15.50	16.44
90	100.00	100.00	100.00	0.00	0.00	0.00	100.00	100.00	100.00

(f) For rays from 90°-112.5° & 247.5°-270° azimuth angles

Incident angle (°)	Front reflectance (%)			Transmittance (%)			Back reflectance (%)		
	1st *	2nd *	3rd *	1st	2nd	3rd	1st	2nd	3rd
75	25.77	5.58	16.43	68.74	84.96	74.79	25.77	5.58	16.43
80	39.76	30.37	40.14	55.73	46.17	36.78	39.76	30.37	40.14
90	100.00	100.00	100.00	0.00	0.00	0.00	100.00	100.00	100.00

1st means the equivalent layer for the front three layers;
2nd means the equivalent layer for the air cavity containing a CCPC-PV structure;
3rd means the indoor glass layer.

Appendix 2. Validation of the building simulation method

The CFD model and ray-tracing model used in the thermal and optical modeling of the original CCPC-PV window, as discussed in **Sections 2.1 and 2.2**, have been validated through indoor testing. This testing was conducted using a spectrometer and solar simulator, as detailed in our recent work by Li et al (2023) [46]. In addition, the performance of the ELFM, which represents the CCPC-PV window in EnergyPlus, has been compared with that of the validated original CCPC-PV window model under various outdoor boundary conditions. This comparison ensures the accurate integration of the CCPC-PV window's properties into building performance simulations, as illustrated in **Sections 2.1.3, 2.1.4, 2.2.3 and 2.2.4**. To validate the building simulation models in **Sections 2.4.2 and 4.2** (excluding the complex window model), another numerical model was developed using the same methodology outlined in those sections. However, this model was created under identical conditions, including building geometry, materials, single clear glass, occupant/equipment schedules, etc., as detailed in [55], specifically under Hong Kong climate conditions. Fig. A2-1 illustrates comparable results between the two simulations, showing annual energy consumption for heating, cooling, and lighting of a building with single clear glass within a 1 % deviation. The validations conducted for the thermal and optical models of the complex fenestration system, as well as the building simulation model within EnergyPlus, demonstrate confidence in the developed method for integrating a complex fenestration system into building simulation software for performance characterisation.

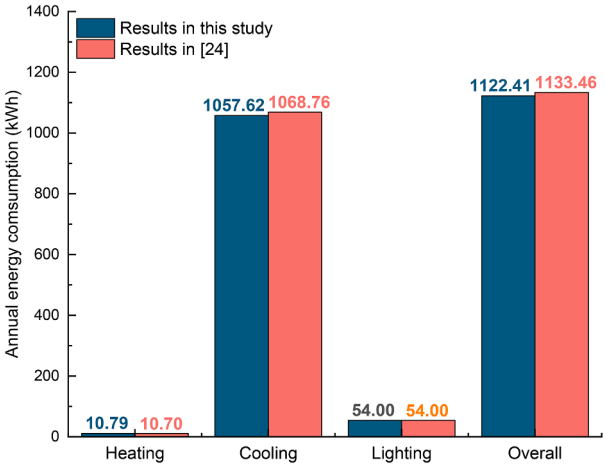

Fig. A2-1. Annual energy consumption of building with single clear glass.

Data availability

No data was used for the research described in the article.

References

[1] X. Cao, X. Dai, J. Liu, *Building energy-consumption status worldwide and the state-of-the-art technologies for zero-energy buildings during the past decade*, Energ. Buildings 128 (2016) 198–213.

[2] X. Wang, C. Huang, Z. Zou, *The analysis of energy consumption and greenhouse gas emissions of a large-scale commercial building in Shanghai, China*, Adv. Mech. Eng. 8 (2016).

[3] O. Chehab, *The intelligent façade photovoltaic and architecture*, Renew. Energy 5 (1) (1994) 188–204.

[4] D.-K. Bui, et al., *Enhancing building energy efficiency by adaptive façade: A computational optimization approach*, Appl. Energy 265 (2020) 114797.

[5] M. van Roosmalen, A. Herrmann, A. Kumar, *A review of prefabricated self-sufficient facades with integrated decentralised HVAC and renewable energy generation and storage*, Energ. Buildings 248 (2021) 111107.

[6] R. Liang, et al., *Evaluation of the thermal and optical performance of thermochromic windows for office buildings in China*, Energ. Buildings 176 (2018) 216–231.

[7] Y. Sun, et al., *Development of a comprehensive method to analyse glazing systems with Parallel Slat Transparent Insulation material (PS-TIM)*, Appl. Energy 205 (2017) 951–963.

[8] B.P. Jelle, et al., *Fenestration of today and tomorrow: A state-of-the-art review and future research opportunities*, Sol. Energy Mater. Sol. Cells 96 (2012) 1–28.

[9] A. Gustavsen, et al., *State-of-the-art highly insulating window frames–Research and market review*. 2007: Norges byggforskningsinstitutt.

[10] J.W. Lee, et al., *Optimization of building window system in Asian regions by analyzing solar heat gain and daylighting elements*, Renew. Energy 50 (2013) 522–531.

[11] X. Liu, Y. Wu, *Experimental characterisation of a smart glazing with tuneable transparency, light scattering ability and electricity generation function*, Appl. Energy 303 (2021) 117521.

[12] N. Yamada, et al., *Performance of see-through prism CPV module for window integrated photovoltaics*, Opt. Express 19 (S4) (2011) A649–A656.

[13] R.-T. Chen, J.L.H. Chau, G.-L. Hwang, *Design and fabrication of diffusive solar cell window*, Renew. Energy 40 (1) (2012) 24–28.

[14] Y. Wu, et al., *Smart solar concentrators for building integrated photovoltaic façades*, Sol. Energy 133 (2016) 111–118.

[15] L.A.A. Bunthof, et al., *Impact of shading on a flat CPV system for façade integration*, Sol. Energy 140 (2016) 162–170.

[16] M. Sabry, Y.A. Abdel-Hadi, A. Ghitas, *PV-integrated CPC for transparent façades*, Energ. Buildings 66 (2013) 480–484.

[17] A. Zacharopoulos, et al., *Linear dielectric non-imaging concentrating covers For PV integrated building facades*, Sol. Energy 68 (5) (2000) 439–452.

[18] W. Lu, Y. Wu, P. Eames, *Design and development of a Building Façade Integrated Asymmetric Compound Parabolic Photovoltaic concentrator (BFI-ACP-PV)*, Appl. Energy 220 (2018) 325–336.

[19] Q. Xuan, et al., *Design, optimization and performance analysis of an asymmetric concentrator-PV type window for the building south wall application*, Sol. Energy 193 (2019) 422–433.

[20] N. Sellami, T.K. Mallick, *Optical efficiency study of PV Crossed Compound Parabolic Concentrator*, Appl. Energy 102 (2013) 868–876.

[21] H. Baig, et al., *Performance analysis of a dielectric based 3D building integrated concentrating photovoltaic system*, Sol. Energy 103 (2014) 525–540.

[22] E.D. Mammo, N. Sellami, T.K. Mallick, *Performance analysis of a reflective 3D crossed compound parabolic concentrating photovoltaic system for building façade integration*, Prog. Photovolt. Res. Appl. 21 (5) (2013) 1095–1103.

[23] K. Allen, et al., *Smart windows—Dynamic control of building energy performance*, Energ. Buildings 139 (2017) 535–546.

[24] Y. Tan, et al., *Parametric study of venetian blinds for energy performance evaluation and classification in residential buildings*, Energy 239 (2022) 122266.

[25] M. Wang, et al., *Comparison of energy performance between PV double skin facades and PV insulating glass units*, Appl. Energy 194 (2017) 148–160.

[26] X. Liu, Y. Wu, *Numerical evaluation of an optically switchable photovoltaic glazing system for passive daylighting control and energy-efficient building design*, Build. Environ. 219 (2022) 109170.

[27] Y. Sun, et al., *Numerical investigation of a smart window system with thermotropic Parallel Slat Transparent Insulation Material for building energy conservation and daylight autonomy*, Build. Environ. 203 (2021) 108048.

[28] X. Wang, et al., *Daylighting and energy performance of the window with transparent insulation slats in the humid subtropical climate zone*, Energ. Buildings 300 (2023) 113685.

[29] R.F. De Masi, et al., *The role of windows on building performance under current and future weather conditions of European climates*, Energ. Buildings 292 (2023) 113177.

[30] K. Khaled, U. Berardi, *A cross-climate assessment of the visual and energy performance of flexible photochromic films for in-situ window retrofits*, Energ. Buildings 300 (2023) 113664.
[31] Y. Sun, et al., *Thermal evaluation of a double glazing façade system with integrated Parallel Slat Transparent Insulation Material (PS-TIM)*, Build. Environ. 105 (2016) 69–81.
[32] X. Liu, Y. Wu, *Design, development and characterisation of a Building Integrated Concentrating Photovoltaic (BICPV) smart window system*, Sol. Energy 220 (2021) 722–734.
[33] Y. Sun, Y. Wu, R. Wilson, *A review of thermal and optical characterisation of complex window systems and their building performance prediction*, Appl. Energy 222 (2018) 729–747.
[34] EnergyPlus, *Engineering reference.* 2019.
[35] A. McNeil, et al., *A validation of a ray-tracing tool used to generate bi-directional scattering distribution functions for complex fenestration systems*, Sol. Energy 98 (2013) 404–414.
[36] H. Yang, et al., *Modeling and analyzing the optical and thermal performance of window with transparent insulation slats*, Energ. Buildings 277 (2022) 112567.
[37] Y. Sun, et al., *Integrated semi-transparent cadmium telluride photovoltaic glazing into windows: Energy and daylight performance for different architecture designs*, Appl. Energy 231 (2018) 972–984.
[38] J. Peng, et al., *Developing a method and simulation model for evaluating the overall energy performance of a ventilated semi-transparent photovoltaic double-skin facade*, Prog. Photovolt. Res. Appl. 24 (6) (2016) 781–799.
[39] W. Zhang, L. Lu, A. Song, *Comparison of the overall energy performance of semi-transparent photovoltaic windows and common energy-efficient windows in Hong Kong*, Energ. Buildings 128 (2016).
[40] H. Musameh, et al., *Energy performance analytical review of semi-transparent photovoltaics glazing in the United Kingdom*, J. Build. Eng. 54 (2022) 104686.
[41] M. Wang, et al., *Analysis of energy performance and load matching characteristics of various building integrated photovoltaic (BIPV) systems in office building*, J. Build. Eng. 96 (2024) 110313.
[42] X. Li, et al., *Comprehensive investigation of a building integrated crossed compound parabolic concentrator photovoltaic window system: Thermal, optical and electrical performance*, Renew. Energy 223 (2024) 119791.
[43] EnergyPlus, *engineering reference*.
[44] *BS EN 673:2011: Glass in building. Determination of thermal transmittance (U value). Calculation method*. 2011, British Standards Institute.
[45] Y.B. Yoon, D.S. Kim, K.H. Lee, *Detailed heat balance analysis of the thermal load variations depending on the blind location and glazing type*, Energ. Build. 75 (2014) 84–95.
[46] X. Li, et al., *Development of a comprehensive method to estimate the optical, thermal and electrical performance of a complex PV window for building integration*, Energy 294 (2024) 130251.
[47] K. Shanks, et al., *An experimental analysis of the optical, thermal and power to weight performance of plastic and glass optics with AR coatings for embedded CPV windows*, Sol. Energy Mater. Sol. Cells 200 (2019) 110027.
[48] D.K. Edwards, *Solar absorption by each element in an absorber-coverglass array*, Sol. Energy 19 (4) (1977) 401–402.
[49] J.L. Wright, N. Kotey, C. Barry, *Solar absorption by each element in a glazing/shading layer array*, ASHRAE Trans. 112 (2006) 3–12.
[50] Ministry of Housing, C.a.L.G., *Approved Document L, Conservation of fuel and power, Volume 2: buildings other than dwellings, 2021 edition.* . 2021.
[51] M. Mirsadeghi, et al., *Review of external convective heat transfer coefficient models in building energy simulation programs: implementation and uncertainty*, Appl. Therm. Eng. 56 (1) (2013) 134–151.
[52] S. Abolghasemi Moghaddam, N. Simões, M. Gameiro da Silva, *Review of the experimental methods for evaluation of windows' solar heat gain coefficient: From standardized tests to new possibilities*, Build. Environ. 242 (2023) 110527.
[53] A. Khaled Mohammad, A. Ghosh, *Exploring energy consumption for less energy-hungry building in UK using advanced aerogel window*, Sol. Energy 253 (2023) 389–400.
[54] K.J. Butcher, *Environmental design : CIBSE guide A / editor, Ken J. Butcher*. Seventh edition. ed. 2006: London : CIBSE.
[55] M. Wang, et al., *Assessment of energy performance of semi-transparent PV insulating glass units using a validated simulation model*, Energy 112 (2016) 538–548.